December 2013

Kilohertz electro-optics for remote sensing of insect dispersal

Sandra Török

Division of Combustion Physics
Lund University

Master of Science Thesis

Kilohertz electro-optics for remote sensing of insect dispersal

LUNDS UNIVERSITET

Master Thesis

Sandra Török

Thesis advisor: Dr. Mikkel Brydegaard

Division of Combustion Physics at Lund University
Lund University Mobile Biosphere Observatory (LUMBO)
Lund Laser Centre (LLC)
Applied Molecular Spectroscopy and Remote Sensing (AMSRS)
Center for Animal Movement (Canmove)
Department of Biology at Lund University

December 27, 2013

Lund Reports on Combustion Physics, LRCP-171
ISNR LUTFD2/TFC-171-SE
ISSN 1102-8718
Lund, Sweden, December 2013
Sandra Török
Division of Combustion Physics
Department of Physics
Faculty of Engineering LTH
Lund University
P.O.Box 118
S-221 00 Lund, Sweden

To my loving mother and father.

Abstract

This thesis evaluates the possibilities of determining the flight direction of insects by analysing the wingbeat modulation pattern of the backscattered sunlight from insects. The Lund University Mobile Biosphere Observatory (LUMBO) was used during the summer of 2013 for a field campaign at two locations in Skåne, Sweden. The purpose of the campaigns was to study insect activity and biodiversity in the natural habitat of the insects, but also controlled insect releases were made. During controlled measurements of known insects, three dimensional flight trajectories were obtained by the use of a high-speed camera together with a strategically located mirror. Also the backscattered sunlight from insects was detected using two four-segmented photodiodes (Si and InGaAs) during dark-field measurements. In this thesis the photodiode data will play a central role. A simple model for the optical cross section (OCS) of an insect is introduced. It describes how the backscattered sunlight will be modulated depending on the angle of observation relative to the orientation of the insect. The signal is modulated with a fundamental frequency and its overtones, which are interpreted as the result of the wing motion of the insect. Assuming that the insects examined follows the wingbeat pattern described in the insect model, the harmonic frequency components of the modulated backscattered light are analyzed by studying their relative intensity, but also the phase difference between them. Three insect signals are examined and in two out of three cases there are some indications that the insect changes orientation during detection, and thereby, flight direction.

Acknowledgements

First of all, I want to thank my supervisor Dr. Mikkel Brydegaard who has helped me, inspired me and supported me throughout these months of thesis work. Also, thank you Igor Buzuk for helping me with circuits and solding, thank you Rutger Lorensson for construction ideas, thank you Minna Ramkull for your helpfulness, thank you Adam Bäckman and Alem Kindeya Gebru for good camping times, thank you Carsten Kirkeby and Ádám Egri for mosquito- and horse fly times, thank you Annika Söderman and Maren Wellenreuther for bumblebee expertise and insect inspiration, thank you Joakim Bood for taking your time to read, thank you Klaes Erixon for listening again and again and thank you Dina Hot, Panagiota Stamatoglou and Jianfeng Zhou for crazy times in E324.

Contents

Chapter 1

Introduction

1.1 Background

In 1955 I. R. Richards, whom exposed Cesium photoelectric cells to direct sunlight would detect, to use his own words, 'bursts'. As the source of these bursts was not visible to the human eye but would reappear from time to time he suggested that this has to be insects flying by, generating a modulated signal due to the oscillating wings. He also went through with some controlled laboratory observations of this phenomena. In his article in *Nature* he wrote in such a suiting way [1]

> "This phenomena is reported here because it seems possible it might be turned to account by workers interested in the flight habits of insects, and particularly in variations in insect density during daylight hours."

As Richards suggests, this is an interesting method for insect detection and scientists have developed similar optical and radar methods, but also acoustic methods to try to obtain better knowledge about insects and their interaction and impact on the surrounding world. A simple, yet elegant experiment was followed out by A. Moore and R. H. Miller *(2002)*, measuring the wingbeat modulations of insects with a setup of insects in a transparent cookie jar, illuminated by a light source from beneath and a photo detector connected to the audio input of a computer. This would allow them to detect the backscattered light, modulated from the wings and so they could compare the wingbeat frequency of different aphids [2].

There does not seem to be much activity when it comes to the development of optical methods for insect detection apart from Lund, and in Montana, U.S.A., where there is a group working with land mine detection using trained honey bees which seek for unexploded ordnance in risk areas. The bees are trained as they are fed with nutrition mixed with explosives and as they have olfactory capabilities down to a single molecule, they will make good detectors. By

being able to detect the spread of honey bees over a minefield by detecting the characteristic modulated backscattered light using LIDAR, the spread can be mapped and so, indicate the position of land mines [3, 4]. This kind of remote insect detection system might also, similar to what I. R. Richards wrote, be of interest to people not just involved with mine sweeping but also to the people interested in the insects themselves.

Optical methods in the area of insect detection by wingbeat modulation observation are attractive as it is both non-intrusive[1]. and can be used for remote sensing. This method has been used by a group of scientists interested in how the detection of trained bees can be used for human needs but in Lund these kind of methods are instead used for research regarding the insects from a biological and ecological point of view.

Lund University Mobile Observatory (LUMBO) is a further development of insect-detecting methods for biological and ecological purpose by the Lund group [7] which has previously worked with similar setups. It is an attempt to use all the knowledge received from these earlier field campaigns to build something that is an optimized and more complete version of all its predecessors, such as the LIDAR-bus or the setup used in Klingavälsån where dark-field spectroscopy was used for insect interaction monitoring [7].

1.1.1 Project LUMBO

LUMBO, the Lund Mobile Biosphere Observatory is a project supported by CanMove (Center for Animal Movement Research), a research platform developed by Mikkel Brydegaard especially for remote sensing of small flying insects and tracking of migrating birds. It is as the name indicates a mobile observatory which can be placed anywhere, as in the case of its predecessor, the LIDAR bus [8]. During daytime it can be used for dark-field measurements and at night time it can be used either for CW-LIDAR or detection and tracking of nocturnal[2] migrating birds. It is a tool for scientists to study the dynamics, characteristics and behavior of birds and insects.

The observatory was built during the spring/summer of 2013 and made its maiden voyage in June-July 2013 to the countryside of summer Skåne where it was used in two field campaigns, the pilot projects. The first field campaign was in Brunnslöv and the second one was at the research field station of the biology department in Lund, called Stensoffa, see figure 1.1.

[1] In active remote sensing LUMBO uses a laser which does not coincide with the visual region of insects (some beetles though, which actively seek for forest fires, have been shown to have infrared detectors [5]). Bees and bumblebees for example, have photo receptors in the UV, blue and green region [6].

[2] Active during night time.

Figure 1.1: Location of the two field campaigns, Brunnslöv (55.7375, 13.6291) during the 24.06.2013-09.07.2013 and Stensoffa (55.6950, 13.4470) during the 12.07.2013-22.07.2013 [9].

1.1.2 Outline and aim of this thesis

The aim of this thesis is to investigate the possibilities of remote sensing of insects and to look into the potential of flight direction identification by passive detection of the backscattered sunlight from insects.

In the beginning of this thesis some important concepts and ideas will be presented in order for the reader to be able to understand why the experiments are outlined as later to be read and to start to create an understanding for the theme of this thesis. The method will be presented by an introduction of LUMBO from a technical point of view, after which the experimental results will be presented along with the evaluated results connected to previously presented theory and models. There will be a discussion following with conclusions and a row of suggestions for the future adventures of LUMBO.

Chapter 2

Theory

2.1 Passive measurements in remote sensing

Remote sensing allows us to gain information from a distance. If a sufficient setup is used, light can be detected and evaluated and eventually tell something about the physical appearance or the chemical constituents of the target. The light source used to illuminate the target will determine how the detected signal will appear.

Passive remote sensing, compared to active remote sensing[1], uses natural radiation sources such as the sun. The sun, a broadband light source which on a cloudless day is continuous and stable will give a stronger signal than e.g. the moon. The radiation from the sun which, apart from the absorbance of the earths atmosphere, is of Planck radiation at the temperature of $5780K$ [10, 11, 12].

In passive remote sensing, usually the light source and the detector are not located at the same place, whilst in the active case they are. In the passive case the angle θ which might change with the time of the day is illustrated in figure 2.1a. In active remote sensing this angle θ is very small and remains the same for all times for the LUMBO setup, this is shown in figure 2.1b. This is important when looking at larger particles, objects or surfaces which might have an asymmetrical optical cross section (OCS).

[1] In active remote sensing a radiation source such as a laser can be used, as e.g. when LIDAR measurements are preformed.

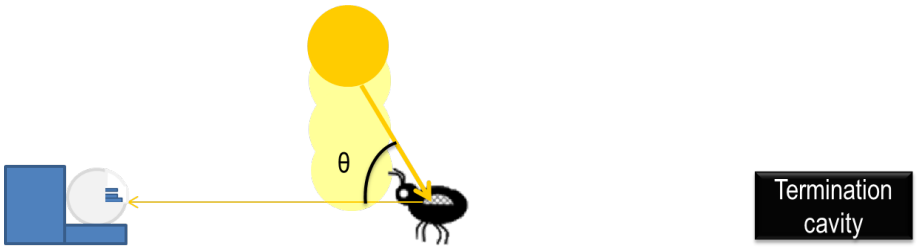

(a) Passive.

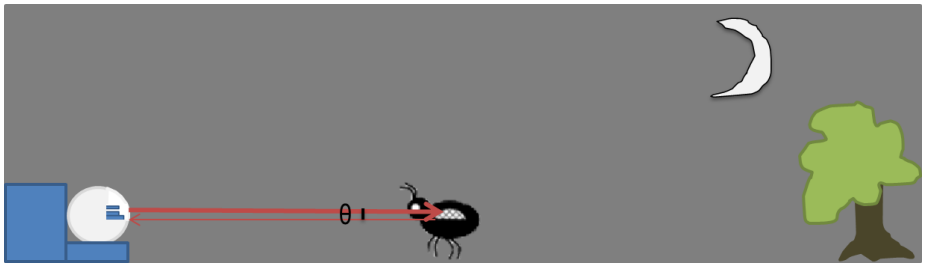

(b) Active.

Figure 2.1: Passive and active emote sensing. Note how the angle θ between the light source and the detector is different in the two cases.

2.2 Physics in entomology

When insects and insect colonies are to be studied, it would involve keeping track of multiple individuals in order to get an idea about insect dynamics, interaction, variety, features, diversity and so on, many things not so obvious even for the trained eye. By using facilities such as LUMBO, which can produce large quantities of useful data, the scientist can get one step closer to answers that has not yet been answered.

By studying the backscattered signal obtained from an insect, the amount of backscattered light and the signal modulation can give information about body size, wingbeat frequency, possibly flight direction and location[2]. That kind of information can be used to characterize insects and to determine species, gender and age [13] of insects which has not been identified in advance. This would allow entomologists in all fields to detect and observe insect activity remotely during long periods of time and so, obtain great statistics of specific species or groups of insects. For scientists this would be interesting when looking at insect behavior, as one group at Lund University who is interested in studying the behavior of see-weed flies in a population which has a mutated gene causing some individuals to grow multiple times larger than normal size. For this group it would be of interest to be able to study a whole colony.

[2]Location can be obtained with the use of the LIDAR setup.

As see-weed flies tend to live in swarms of hundreds of flies in a relatively small volume, it makes it very hard to collect data manually by counting and observing [14]. And for Lauren J. Cator and her group at Cornell University in Ithaca, USA, who used an acoustic method to study mosquitoes in Thailand. They specifically studied their wingbeat modulation, the phenomena called 'harmonic convergence'[3] and their role as a disease-vector [15]. The study of insects can be of great importance when looking at insect-borne diseases, because by studying the behavior of the insect, the epidemiology is better understood. A vector-borne disease such as malaria killed about 660 000 people in 2011 [16]. It is a huge problem, especially in Africa and might be somewhat easier to control if the behavior of the mosquitoes were mapped better. Other diseases carried by insects might be different pests, not striking against humans, but towards crops and livestock essential to humans. In some cases it might be interesting to study the direction of flight relative to the wind. Insects with 'hosts' such as cattle, might have different strategies to find them. Would the insects fly with the wind and save energy? Will they travel transversely with the wind for largest chance to encounter a CO_2 plume and then against the wind when knowing the direction of the plume?

2.3 Insects in different spectral bands

Detectors used during the field campaign respond to different spectral bands (see section 3.1.2). This means that an insect might look different as it is detected by a Si photodiode, than as it is detected with a InGaAs photodiode, depending on the properties of the insect body and wings. Looking at the body of an insect it is usually colored strategically for survival. A common strategy would be to have melanin in the curticle, as it absorbs well in the VIS and NIR region and hence heats the insect, which can be beneficial to certain extents [11]. The wings on the other hand are chitinous membranes. Depending on the background and the orientation of the incoming light, these wings might appear very different. As presented in Mikkel Brydegaards thesis (*2012*), the angle of observation and wavelength of light source is crucial when looking at the reflectance of the wing [17].

2.4 Insect model

A simplified wingbeat cycle of an arbitrary diptera[4] insect is presented in figure 2.2. The wing appears large at one occasion during a wingbeat cycle seen from above and from the front, from the side it appears to be large twice during one cycle [18]. A flying insect seen from the front or the side would then generate a modulated signal with the fundamental frequency (1ω), while

[3] This phenomena describes how a female and male mosquito change their wingbeat frequency to match some of their harmonic frequency component, a possible way of finding a mate.

[4] An insect with two wings, meaning one pair of wings.

from the side there would be the second harmonic (2ω), meaning twice the fundamental. The body, which does not give rise to any modulation will be a DC signal which is large from the side and above, but small from the front.

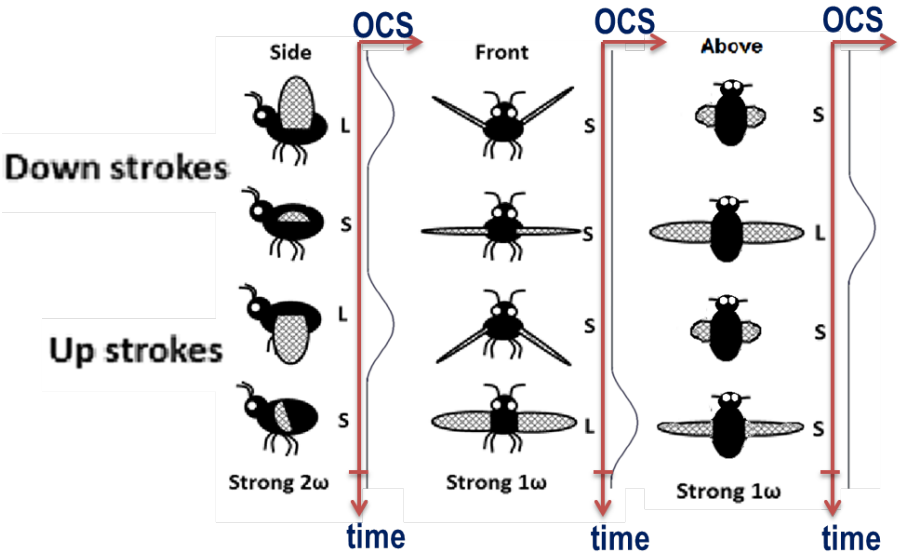

Figure 2.2: Wingbeat cycle and the orientation dependent harmonic content.

In figure 2.3 the harmonic frequency components contributions to the insect signal depending on the orientation are presented. *DC* and 1ω will have the shape of a plate as it contributes in two planes, 2ω appear as an ellipsoid as it only contributes in one plane. The sum of these frequency components describes the total OCS of the insect model.

The backscattered light from an insect will be modulated according to the insect model. In frequency domain the modulated signal can be described with a set of harmonics (as 1ω and 2ω). This means that the OCS of an insect is time dependent. But the amount of backscattered light also depends on the spectral range of the light source, the detectors and on the orientation of the insect (indicated in figure 2.2). So, the OCS is time-, wavelength- and orientation dependent.

If one would create the same kind of model, but for a dragonfly (which has four wings), it will become more complicated. It should be noted though that in this kind of model the number of wings is not necessarily the factor that determines the complexity of the relation between the harmonics that describes a certain insect.

This particular model shows that the relative strength of the odd and even harmonics of the OCS can be used to determine the orientation of the insect and thereby perhaps its heading direction.

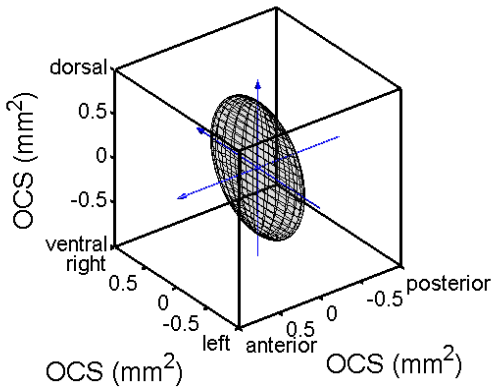

(a) DC.

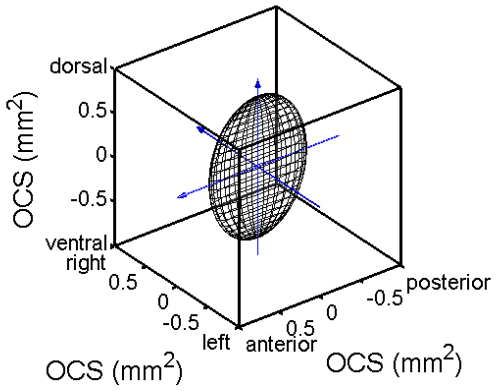

(b) 1ω.

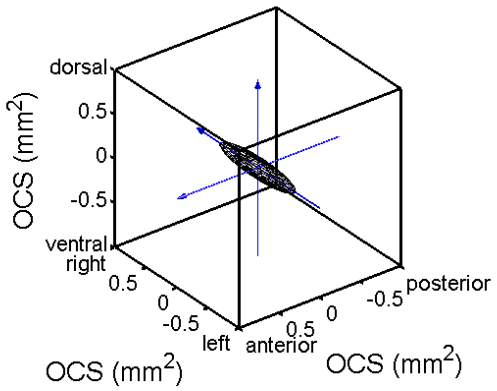

(c) 2ω.

Figure 2.3: The contribution to the OCS depending on the direction of observation for a simple insect.

2.5 Form Factor

The intensity of the collected light will be a function of the distance for the Newtonian telescope, used along with the quadrants. This dependence, which is also an important part of the traditional LIDAR equation, is also out of interest during the remote sensing measurements. This range dependent function is often mentioned as the geometrical factor, geometrical form factor or, as it will be referred to throughout this thesis, the form factor. It consist of two parts, one part which describes how the signal decreases with distance and the other part which describes the near field signal. See equation 2.1 for the form factor function where G_0 is the constant signal along the optical axis, R is the range of light source and field of view (FOV) overlap (the overlap area), r_0 is the center of the overlap area and r is the distance [11, 19, 20].

$$G(r) = \frac{G_0(1 + tanh(\frac{r-r_0}{R}))}{r^2} \tag{2.1}$$

2.6 Dark-field

During dark-field measurements, which implies optically zero background measurements, there should be no background signal in the ideal case. If measurements are made where air is present in the FOV though, effects such as scattering of air is something that is unwanted and hard to come around. Dark-field measurements can be obtained quite well when trying to detect insects by using a black cavity as a background, so there will not be any other signal than from the insect in the FOV, air scattering and dark current[5]. There are many different ways to terminate a beam or just creating a black background. Blackness is a term that has to be taken into consideration when using a detector of a certain spectral band. A material of high absorption in the spectral region of interest is crucial in order to obtain a sufficient black cavity in order to be able to detect the signal of small insects. Also the design of the cavity can be optimized by trapping the entered light which causing the light to bounce multiple times n and thereby absorbing A^n (A is the absorbance) of the total incoming light [22].

2.7 Optical cross section

The optical cross section (OCS) of an object describes its ability to reflect light. How much is reflected back depends on its reflectivity and on the source of illumination. To obtain the OCS of an object in a specific wavelength range, one should use a detector of a matched spectral range which is calibrated[6]. It

[5] Noise which is due to thermal effects causing random electron-hole pairs in the p-n junction of a photodiode [21].

[6] Detection with e.g. a photodiode would give a signal where the unit is V, this can be converted to mm^2 by calibration.

can be calibrated by using the detector to measure objects of known size which is known to be white in the chosen spectral range.

For objects such as spheres of uniform shape, material and surface, the OCS will be the same for the entire body even if it is rotated relative to the light source and the detector. For objects such as insects which are only somewhat symmetrical through their saggital plane, the OCS will strongly depend on the orientation in space relative to the light source and the detector. As the insect flies, the OCS will also depend on the wingbeat cycle. So there is in this case a wavelength-, orientation-, phase- and time dependence of the OCS. This can be compared to radar cross section (RCS) which is a more common expression, used in the radar context as a measure of the backscatter efficiency [23].

Chapter 3

Methods

During the field campaign at Stensoffa (55.69501, 13.44702) LUMBO is situated facing north. In figure 3.1 an overlook of the of external equipment is presented, the calibration box and the calibration pendulum situated about half-way to the termination cavity. The position of the calibration box (section 3.4) and termination cavity (section 3.3) is chosen so that everything is aligned as good as possible, especially taking into account that the calibration box should be positioned at about hip-height in order to be able to work from underneath it, but also to be able to adjust its lid when needed. Also it is more stable when it is not kept too high.

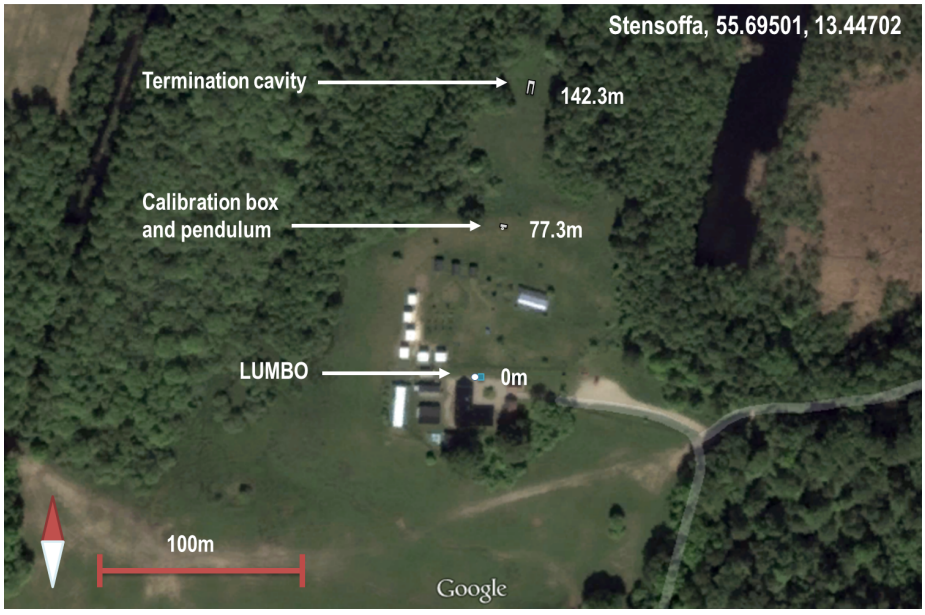

Figure 3.1: The Stensoffa areal view.

3.1 LUMBO instrumentation and setup

LUMBO consists of a control room and a dome. They are connected by a tunnel constructed to guide cables between the computers in the control room and the instruments in the dome, also it allows access to the dome as there is no direct entrance. All of the equipment except the computers are permanently located in the dome. The mount is on a pier, a bit off the center of the dome, and all the telescopes and detectors are attached to this. The mount allows rotation in all directions and it is driven by a motor which is computer controlled and the user can easily rotate the setup with a program with a user friendly interface. The shutter of the dome and the entire dome itself is rotated by motors. Equipment carried by the mount is carefully balanced, allowing the motor to move it easily. The data collecting instruments are listed below.

- Telescope
  - Skywatcher Telescope N 300/1200 Quattro
  - Skywatcher Telescope AC 102/500 Startravel OTA
  - Skywatcher Maksutov telescope MC 102/1300 SkyMax OTA
- Photodiode
  - InGaAs PIN photodiode Hamamatsu (G6849)
  - Si PIN photodiode Hamamatsu (S4349)
- Camera
  - Framos Lumenera LT225 CMOSIS Sensor
  - Spyder3 2k, 18 kHz GigE Line Scan DALSA Teledyne CCD
- Laser
  - O-like diode laser 810 nm
- Spectrometer
  - Ocean Optics spectrometer USB4000
- Weather data
  - Digital Weather Station

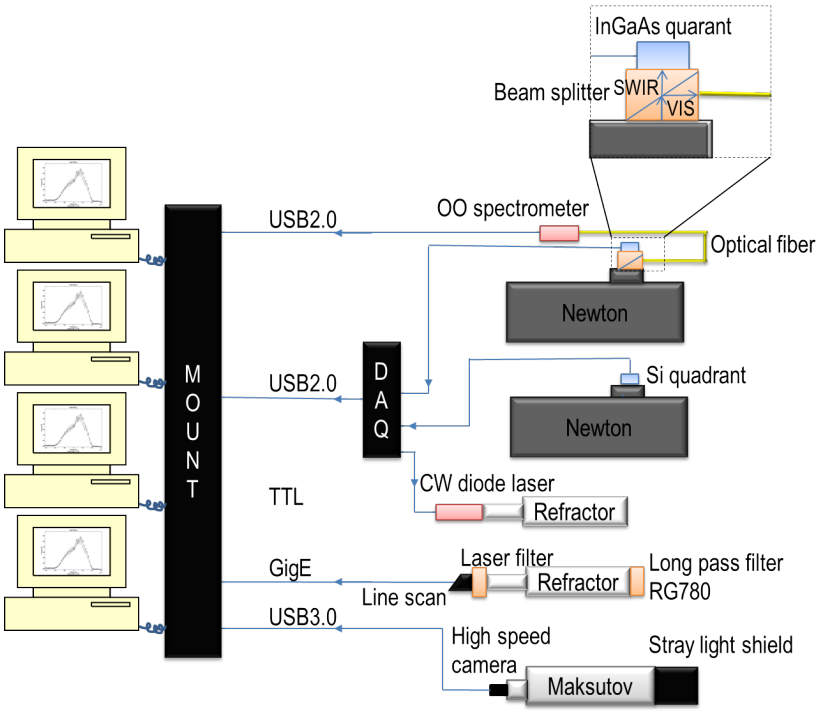

Figure 3.2: Experimental setup with information flow.

In figure 3.2 the entire setup is presented and also one can follow the flow of information. The two large Newtonian telescopes are 'sandwiched' in between two aluminum rails, see figure 3.3. These serve as a surface on which some additional instrumentation can be attached such as analog to digital converters, the DAQ board and spectrometer. As the image shows, the two quadrants used during our field campaign is used together with the Newtonian telescopes whilst the laser is used with a refractor which is also the case for the line scan. The high speed camera is then used with the Maksutov telescope. The main reason for this configuration is that the quadrants need a lot of signal in order for small insects to be detectable and not drown in the noise, so the telescope of largest aperture is chosen. Extensions are added when the detectors are put in position in order to obtain focus where it is wanted. The orientation of the line scan is of great importance when using the LUMBO facility for CW-LIDAR measurements, but this will be further discussed in chapter 3.2.

3.1.1 Telescopes

There are three different telescopes in the LUMBO setup. Two refractors, two Newtonian and one Maksutov. The properties of the telescopes are known in order to be able to e.g. calculate the magnification at certain distances in order

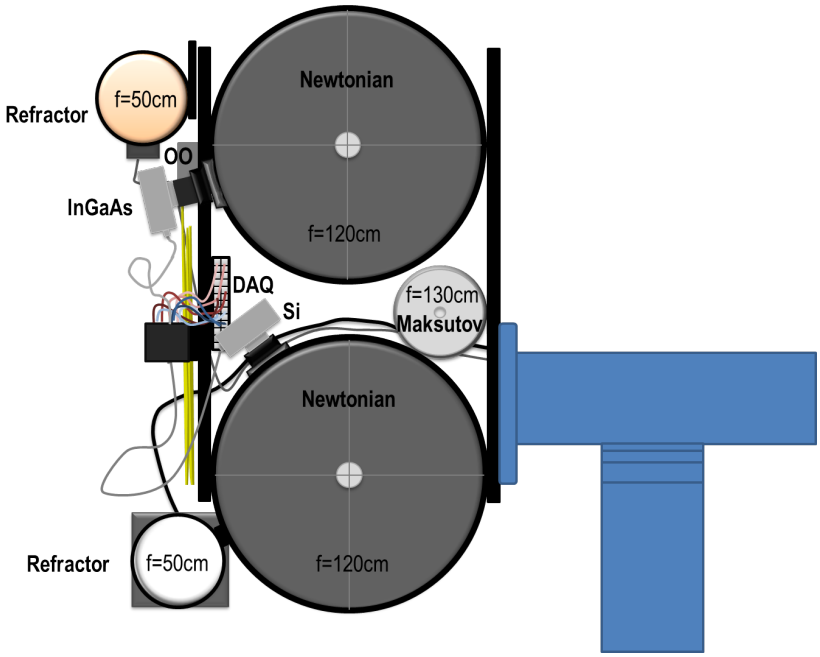

Figure 3.3: Mount construction from the front.

to be able to know the shape of the FOV. As the Newtonian telescopes are the ones used for the experiments in this thesis along with the quadrants, these are the telescopes that will be discussed further. In order to eventually understand why the form factor is as it is, presented in chapter 2.5, the geometry of the Newtonian telescope has to be discussed.

The Newtonian telescope consists of the a tube and two mirrors. One large concave mirror in the bottom of the tube (primary mirror) and one small tilted mirror in the center of the other end of the tube (secondary mirror), the end where light is entering the telescope. The incoming light will fall onto the primary mirror and focus down the light onto the secondary mirror which reflects out the light to the detector located on the side of the telescope. The secondary mirror is situated in the path of the incoming light and so, it will prevent some of the light to make it to detection. The effect is larger in the near field of the telescope and so it is seen, described by the form factor.

3.1.2 Detectors

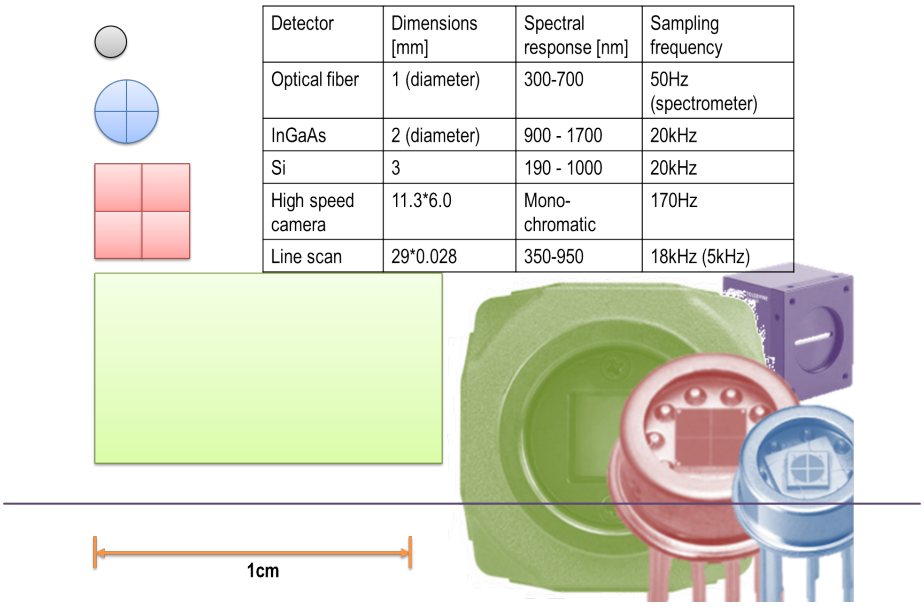

Figure 3.4: Scheme of LUMBO detectors.

The LUMBO setup includes two different segmented photodiodes, all detectors are schemed in figure 3.4. Depending on the semiconductor material in the photodiode, it is sensitive to a certain spectral region. A comparison of the spectral bands is presented in table 3.1. Si and InGaAs are used and so light is detected in NIR and SWIR.

Detector	Spectral response [nm]
Si	190 to 1000
InGaAs	900 to 1700

Table 3.1: The spectral region of detection. [24]

The temporal bandwidth of a photodiode gives the frequency of the detected signal when it has been attenuated 3dB, which corresponds to 70.79%. A signal of higher frequency will be more attenuated and not reflect the true intensity of a signal. The cut-off frequency was experimentally determined by a simple setup of a light emitting diode modulated by a pulse-generator with the photodiode of interest detecting the modulated light, both displayed in an oscilloscope. For both the InGaAs and the Si quadrant which has bandwiths of 2.5 kHz and 2.9 kHz as can be seen in table 3.2, there will be a signal detected even at magnitudes of tens of kHz, but in this case, heavily damped. The experimentally obtained response of the Si and InGaAs detectors are presented in figure 3.5.

Detector	Bandwidth $[kHz]$
Si	2.9
InGaAs	2.5

Table 3.2: The bandwidth.

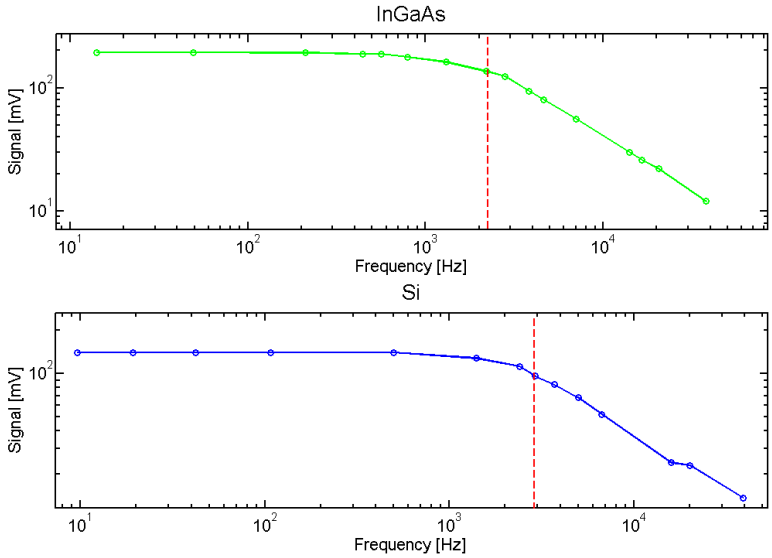

Figure 3.5: The response of the two detectors, red line indicating the cut-off frequency.

In figure 3.6 the phase difference between the generated modulation and the detected modulation is presented. There is no obvious behavior other than a tendency of decreasing with the frequency (note the logarithmic x-axis) , but what should be observed is a *arctan* shape around the cut-off frequency, just as for a low-pass filter. This might be of interest when the phase of different frequency components of a signal is out of interest, which is actually the case in this thesis, but on the other hand there is no use of the frequency components reaching over the cut-off frequency.

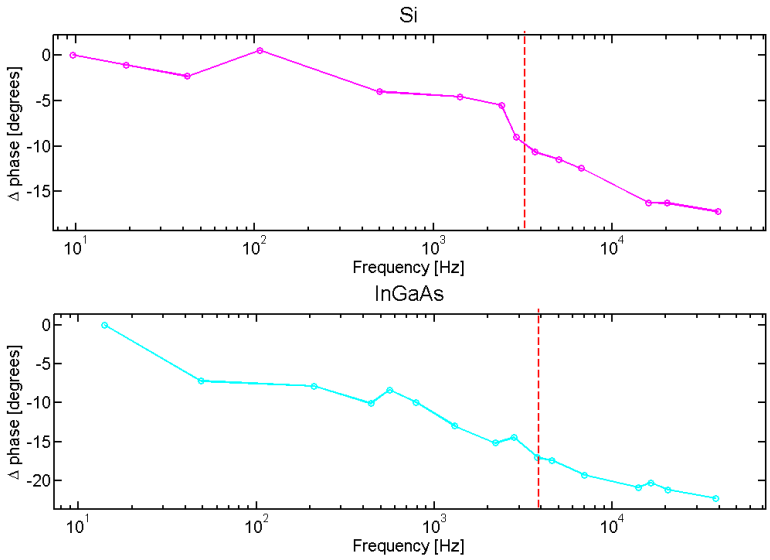

Figure 3.6: The frequency dependent phase difference of emitted modulated light and the detected modulated light. Red line indicating the cut-off frequency.

A CMOS high speed camera is used to image the insect event detected by the other detectors. The main purpose of the camera is to be able to identify the insect signals appearing in the quadrant data. In this thesis the aim is to be able to gather information from the insect signals from the quadrants and describe the heading direction. Together with a 45 degree angled mirror a three dimensional image of the insect flight can be obtained and compared with quadrant data. The high speed camera only records image sequences as it is triggered when something enters the FOV, or there would otherwise be an overload of data (and mostly not useful data). The high speed camera has a sampling frequency of about 170Hz, enough to see the direction of flight but somewhat slow to detect the wingbeat cycle of small insects.

An Ocean Optics spectrometer is attached to the same Newtonian telescope as the InGaAs quadrant. A beam splitter reflects the light in the visible region to the spectrometer.

The LIDAR system of LUMBO consists of a laser and a tilted line scan CCD camera of 2048x2 pixles where the pixels are binned 2x2, hence the measurement will contain 1024 data points in a row. This CCD camera operates in the visible region and all the way up to about 950nm but in the LUMBO setup it is used together with a laser filter suited for a laser at around 810nm. A longpass filter (RG780) is used in order to absorb light in the region of sensitivity of the CCD.

3.2 LIDAR

In Light Detection and Ranging (LIDAR), pulsed lasers are used in order to obtain the range resolved image which is the purpose of LIDAR. But pulsed lasers are more expensive and usually larger than continuous wave (CW) ones. A CW system is an interesting compliment to the pulsed one, but then the range information needs to be obtained using a different method than by taking the duration for the pulse to return to the detector.

By the use of a line scan detector and the implementation of the Scheimpflug principle, allowing one to change the plane of focus (PoF) by letting the detector plane and the subject plane coincide in the plane of the image. This means that the focus of the detection system would be along the laser beam, if the detector is tilted with a suited angle. So each pixel in the detector will represent a range bin. Depending on the focal length of the reciever, the range resolution can be adjusted, given that the Scheimpflug condition is satisfied. A simple setup where the Scheimpflug condition is fulfilled, is presented in figure 3.7 [25].

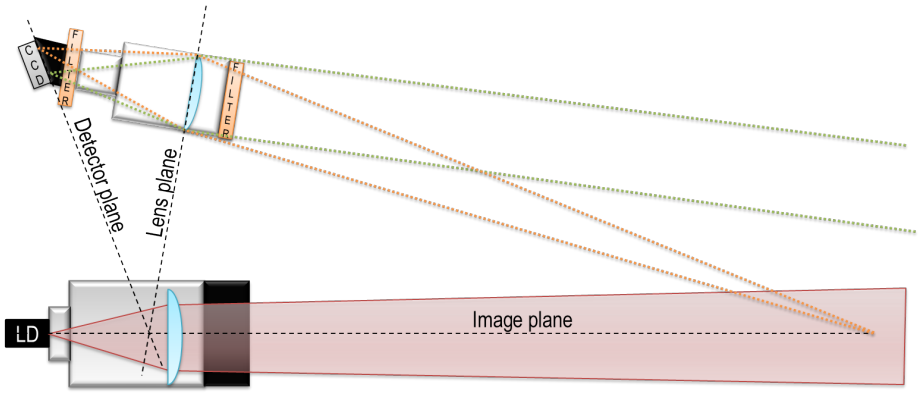

Figure 3.7: The three planes intersect leading to focus along the image plane.

The difficulties of this system arises when trying to obtain an overlap of the laser beam and the line scan detector. In order to preserve as much laser power as possible for detection, the laser beam should be kept as thin as possible, but due to temperature changes during acquisition time, the devices might become unaligned due to thermal expansion during night.

For this CW setup the measurements should be done during night time in order to minimize background signal.

3.3 The termination box

In order to do dark-field measurements a termination cavity is constructed according to chapter 2.6. For LUMBO field campaigns black flute plastic is used whereof a cylinder shaped cavity is constructed, see figure 3.8. Also a

cap is constructed at the opening of the cavity, to prevent direct sunlight from entering the cavity. Inside, there is a bent sheet of plastic which is used to make the incoming light bounce multiple times and thus attenuate it as much as possible

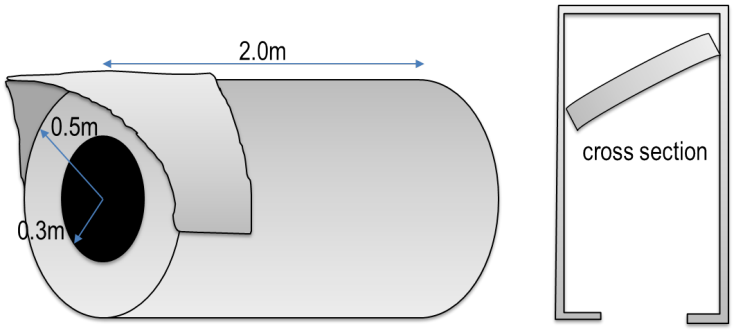

Figure 3.8: Model of black termination cavity.

3.4 The calibration box

The calibration box is used for releasing known insects into the FOV while LUMBO is collecting data. As discussed in chapter 3.1.2, a tilted mirror is needed to image the three dimensional flight trajectory of an insect, as it is flying through the FOV. In figure 3.9 the box is presented seen from above. In one end the mirror is positioned, tilting with 45 degrees[1] and in the other end a small termination cavity is positioned in order to obtain a clear image of the mirrored insect, rather than vegetation or even other insects outside of the box. As the insect flies through the box, it will be mirrored and so the flight trajectory can be obtained from the high speed camera, further details in figure 3.10.

[1] 45 degrees is chosen for easy conversion of coordinates in the mirror plane.

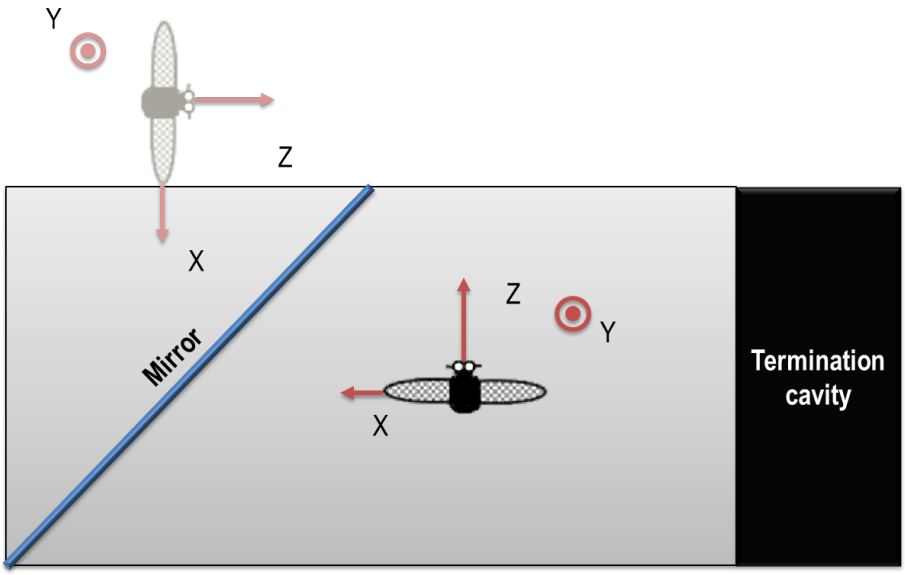

Figure 3.9: Cross section image of the calibration box, illustrating the mirrored coordinates in space.

The dimensions of the box are determined taking some important aspects into consideration. The FOV of the quadrant data should pass through the mirror box without overlapping with some part of the box. If the box would be in the FOV of some quadrant, it will probably be detected as a very slowly oscillating object, as the wind might make it move along with it. It must also be possible to image most of the mirror part of the box and the open part of it with the high speed camera. If the FOV of the camera is larger than the box, it can be adjusted from the triggering program.

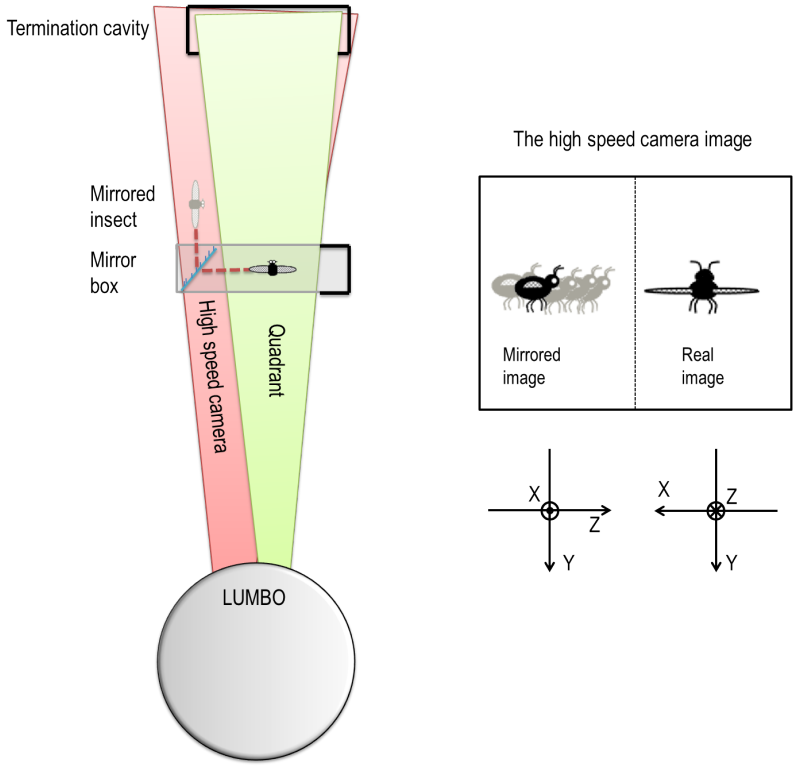

Figure 3.10: The mirror is only in the FOV of the high speed camera. The image of the insect in the FOV is presented on the right side.

Another point is that the ground might not be flat at all out on the countryside, so adjustable tripod legs is a great way to compensate for that. Additionally a lid is made over the open part of the box, making it possible to adjust the direct sun exposure of the insects, and holes are made in the bottom board for insect releases. The calibration box in use is shown in figure 3.11.

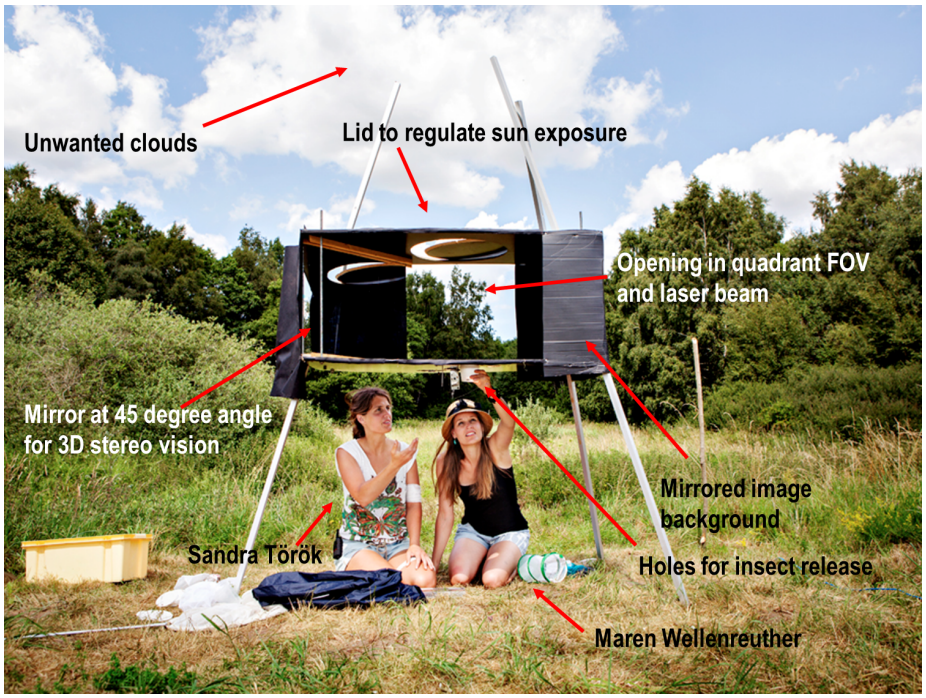

Figure 3.11: The calibration box used by Sandra Török and Maren Wellenreuther. Foto: Sydsvenskan

3.5 Calibration

In order to be able to convert the signal intensity of the quadrant data (which is given in *volts*), to the OCS in mm^2, calibrations needs to be done throughout the entire day of measurements. Calibrations are also done in order to determine the orientation of the quadrants and for possible mirror corrections. Three types of calibration are done:

- a white painted bamboo pendulum, oscillating from one side to the other through the entire FOV, always released from west to east. The procedure is done every half an hour.
- white pressed paper spheres[2] in three different sizes and two out of each size is dropped through FOV in a decided sequence, size given in figure 3.12.
- a b/w checkerboard is moved around in FOV.

[2]Called *flörtkulor* in Swedish, commonly used for arts and crafts.

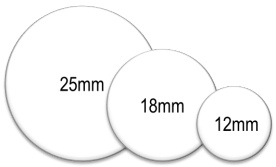

Figure 3.12: Spheres used for white and OCS calibration.

3.6 Experiment conditions

The external conditions for the LUMBO setup has to be optimized in order to obtain the best possible data. When running the system it is known that:

- backscattered light from insects far away is supposed to be detected
- the setup specified in chapter 3.1 which is located in the dome is used
- a termination cavity is used for the dark-field measurements
- a calibration box is used during controlled releases
- the camera is triggering on insects within a chosen FOV

As insects which usually tend to be very small are suppose to be detected, it is important that the insects are exposed to direct sunlight. This is taken into account when constructing the mirror box, which has, as mentioned in chapter 3.4, a removable lid[3]. The fact that direct sunlight is needed is also a reason for the weather dependence of the system. Cloudless days are needed in order to obtain stable and linear signals, see perfect conditions in figure 3.13. During rainy days the dome can not be open. To increase the chance for insect detection, the triggering image chosen for the high speed camera should be as large as possible but not overlap with permanent non static objects such as a moving box caused by a strong wind.

[3]During most of the day the sun is actually not shining from above but it will shine into the box from the front.

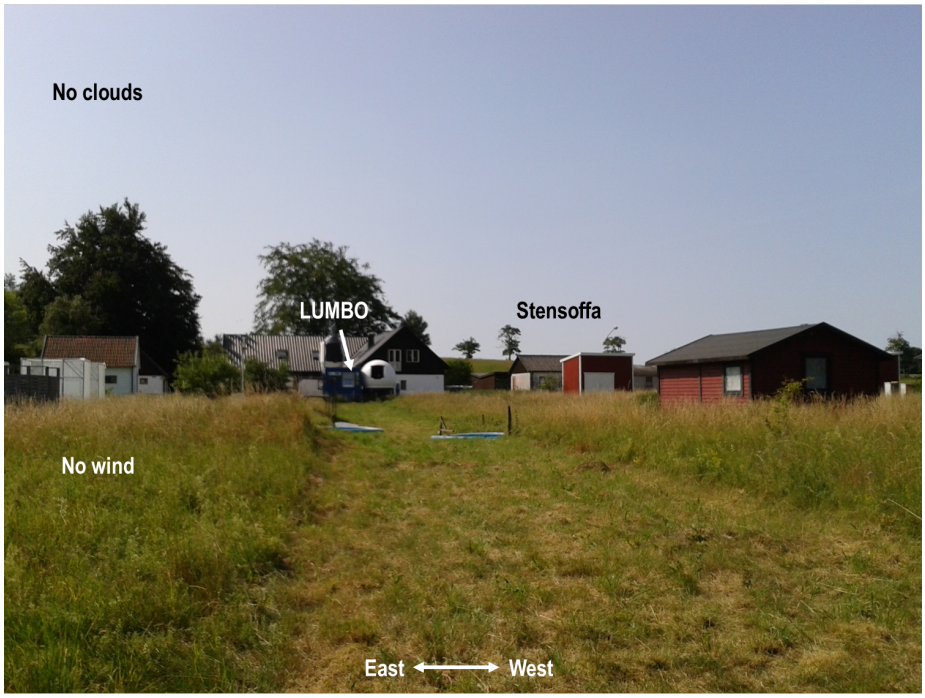

Figure 3.13: The Stensoffa scene.

3.7 Data analyzing

Data is collected all day for a few non cloudy days, this leads to huge amounts of information being collected and stored. In this thesis we only look at some calibration events which are of interest during days of insect releases (20th and 22nd of July) as well as some data files of insect events in quadrant and high speed camera data from another day with good weather (21st of July). As only a few calibration- and insect-events are evaluated, this thesis does not cover the matter of algorithms for classification and such, but nevertheless looks into the information that can be obtained and used as parameters in such evaluation.

3.7.1 Calibration

The pendulum is always released from west to east and enters the entire FOV of each segment equally much, but at different times, depending on the orientation of the quadrant. As the different segments of the detector might not respond equally to the pendulum entering the FOV, there must be some compensation done. By normalizing each signal, dividing by the maximum of each pendulum

signal, the segments will be weighted.[4]

The spheres dropped into the FOV should give equally large signal in each segment as they are weighted, but of course only if the sphere enters the FOV of each segment equally as much. As the spheres usually do not do that, the conversion from voltage (V) to OCS (mm^2) has to be made in some way where this is taken into account. By fitting a square pulse[5] to the signal generated by the sphere, the conversion coefficient can be obtained. This procedure can be done in various ways, preferably optimized for the chosen way of data evaluation.

3.7.2 Signal analyzing

Each data file from the quadrant consists of a 50 second sequence of dark-field remote sensing results. From these, the insect events are investigated (as well as the calibration events, which were discussed in previous chapter). The main information that can be extracted from the quadrant data is listed below.

- body
- modulation frequency
- relative size of the harmonic frequency components (odd, even i.e.)
- relative phase information

In order to get the frequency content of a modulated signal using Matlab, the Fast Fourier Transform (FFT) can be used. As the signal content might not be constant the time dependence should not be forgotten. By using the short-time Fourier transform (STFT) which is also called time-dependent Fourier transform, a window of a certain size and 'shape' is used and swept over the signal as Fourier transform is done over each segment. The STFT is defined in equation 3.1[6] where $x[n]$ is the signal and $\omega[n]$ is the window function [26].

$$X_{STFT}(e^{j\omega}, n) = \sum_{m=-\infty}^{\infty} x[n-m]\omega[m]e^{-j\omega m} \tag{3.1}$$

The magnitude of the STFT is called spectrogram and gives a three dimensional representation of how the frequency content and signal changes with time, see equation 3.2.

$$spectrogram(t, \omega) = |STFT(t, \omega)|^2 \tag{3.2}$$

The window function x used when creating a spectrogram of the obtained raw signal should be of Gaussian shape as the signal is of the detected insects in

[4] This way of compensation for the uneven amplification can of course be done in many ways. If the shape of the segment signals are the same, this simple method is considered sufficiently accurate.

[5] If the signal would be perfect then it would be a square pulse, but due to focus not being perfectly aligned and the response of the detector, it will appear as a Gaussian pulse.

[6] In this form it is called discrete-time STFT.

our case is located in focus, hence the Gaussian profile of the signal should be used as the Fourier transform of the Gaussian will remain the same in frequency domain.

From the spectrogram the relative intensity of the frequency components can be evaluated as the frequency bins are extracted from the data matrix. But as the spectrogram does not contain any phase information, the phase should be extracted by operating the Fast Fourier Transform (FFT) stepwise, using a window which is swept over the signal. Using *angle()* on a certain frequency component it will be given a value between $-\pi$ and π. In order to make a series of phases more smooth, *unwrap()* will add or subtract 2π when there is a step between π and $-\pi$. It is important to acknowledge the fact that even though there might be no change of phase between two consecutive steps, the phase will still, due to the FFT function in Matlab, show that as it obtains the phase from the position of a frequency component relative to the window. If the step between each iteration would be of the period of the interesting frequency component, then of course this problem would not occur. The phase is obtained according to equation 3.3, for each step of the interesting frequency components $f_{n\omega}$, while equation 3.4 shows the compensation vector for a certain frequency component with the frequency $n\omega$ [27].

$$phase = unwrap(phase(FFT(Signal - offset))) \tag{3.3}$$

$$compensation = f_{n\omega} \cdot nbrOfSteps \cdot stepOverlap \cdot \Delta t \tag{3.4}$$

3.7.3 Direction assessment

From the insect model presented in chapter 2.4 we know that the OCS of an insect is dependent on the angle of observation. The information in the signal which can be used in order to determine the direction of flight/orientation is listed below.

- The relative strength of the harmonic frequency components.
- The phase difference between 1ω and 2ω.

At a certain time during an event the signal will be built up by a set of harmonic frequency components. How much of each component is given in the spectrogram of the signal at the given time interval. The relative intensity of the frequency components indicated the direction of flight, by the use of a certain insect model. Using the simple insect model presented in this thesis, the relative intensity of the odd and even frequency component indicates the direction of flight. Also the phase difference of the different frequency component can show such information. In our model though, the relative phase between the fundamental and the first harmonic frequency would be $\pi/2$ for all cases.

The frequency contributions which are visualized in figure 2.3 are simple three dimensional ellipsoids and easy to describe with the formula for

an ellipsoid. However, in reality these representations of the frequency contributions would be more complex but nevertheless a spherical function with associated conditions for continuity. Spherical harmonics are described in appendix A as a complete set of base functions which can be used by linear combination to approximate any continuous spherical function. Spherical harmonics can therefore be used to express the harmonic frequency components for other more complex and realistic insects.

Figure 3.14 shows how the insect specific matrix can be obtained for an insect which has been detected both by the high speed camera and the quadrant. From the high speed camera the position in space is obtained in (x, y, z), from an image sequence the speed can be extracted and when converted to polar coordinates, the speed is given by r. Angle θ and ϕ will be the pitch and jaw of the insect, which describes the heading direction of the insect, indicating the orientation of it, seen from the detector. These angles are then used when a set of even and real harmonics are selected in which the insect specific model can be expressed. From the quadrant the modulated signal is obtained and as it has been calibrated to give the OCS, the harmonic frequency components (1ω and 2ω in this example) and the envelope (DC) can be extracted. As the figure shows, the insect specific model is extracted by solving the system of linear equations $S(\theta, \phi) = H(\theta, \phi)A$, where A is the insect specific model. Using this method one can hope for the insect not just to pass straight through the field of view, but actually do some turns.

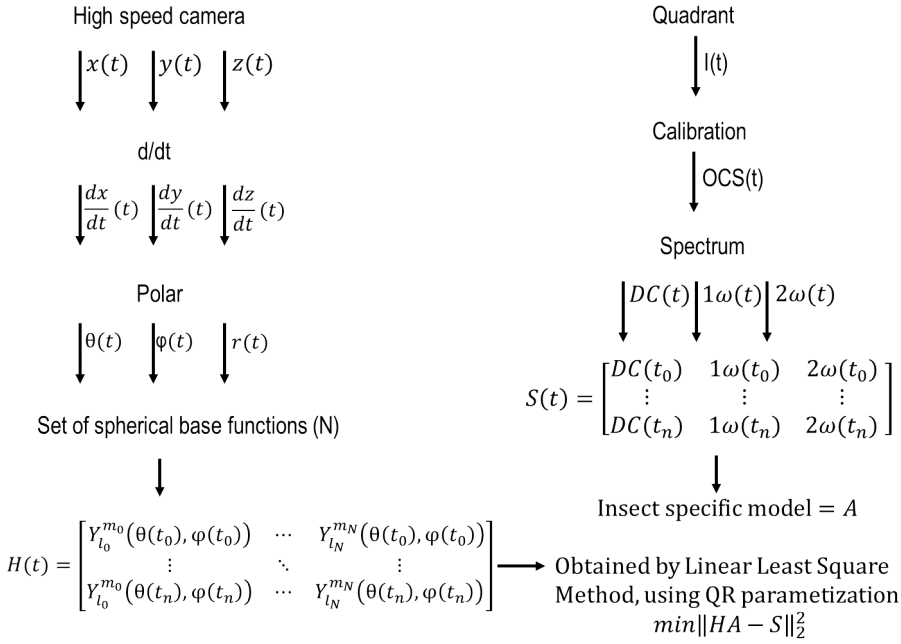

Figure 3.14: Flow chart of how the high speed camera images and quadrant data is used to obtain the insect specific model A [28].

3.8 Image processing

As an insect enters the FOV, the high speed camera will trigger and start recording the insect event. From the image sequence the flight trajectory in two dimensions can always be extracted. The trajectory in space is not known, but by using a mirror as described in chapter 3.4 the third dimension information can be obtain, assuming that the orientation of the mirror relative to the camera is known so that the orientation of the base coordinated are known in the image space compared to their orientation in direct space.

Chapter 4

Results

4.1 Quadrant data

Quadrant data is collected as long as the sun impinges upon all the equipment placed out on the field. During a cloudless sunny day there are in the order of 20000 insects events in the FOV of about $1.95m^2$ in the InGaAs quadrant case, which after just a few days along with spectrometer-, camera- and weather data can most likely excite all insect interested scientists to a higher level of happiness.

4.1.1 Calibration

The signal from a calibration event is presented in figure 4.1 where the first set of fluctuations is a pendulum event lasting for 15 seconds, followed by two large spheres, two medium size ones and two small spheres. The signal intensity is measured in volts.

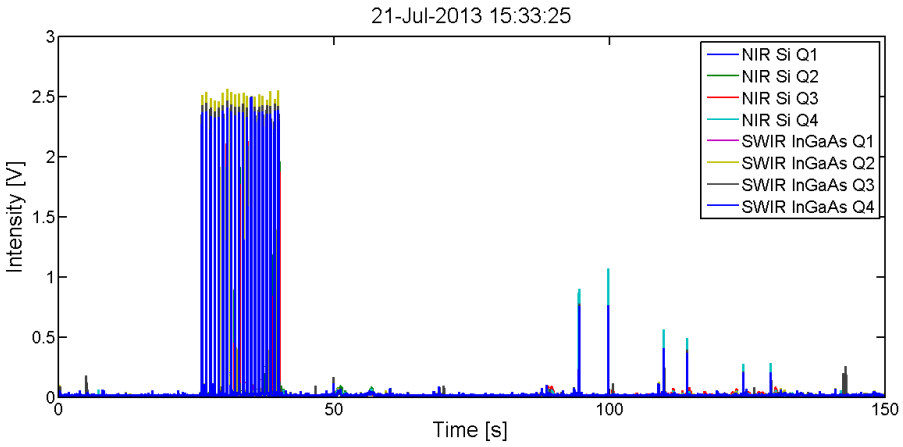

Figure 4.1: Calibration events, no optical cross section.

In figure 4.2a two pendulum sweeps through the FOV are presented. They are mirrored due to the pendulum sweeping through the FOV the same path but in the opposite direction. What can be see more clearly on the zoom-in in on one of the sweeps in figure 4.2b, is that the signal is not equally strong for each segment, which they should be. By weighting as explained in chapter 3.7.1 this can be adjusted and the result is shown in figure 4.3. For each quadrant two segments appear in the signal at the same time, which means that the pendulum enters two segments at the time. First the Si quadrant is entered in segment 2 and 3. After Si quadrant segment 1 and 4 just and the InGaAs quadrant segment 3 and 4 entered. Finally quadrant segment 1 and 2 of the InGaAs is entered. This allows us to suggest a first alignment of the quadrants, see figure 4.4.

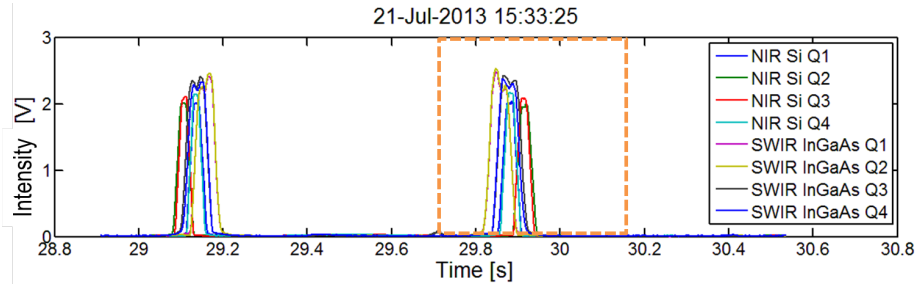

(a) Sweep from west to east and east to west.

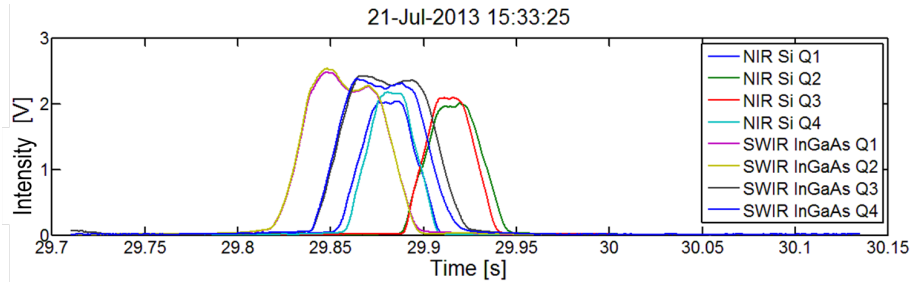

(b) Sweep from east to west.

Figure 4.2: Pendulum sweeps during calibration, *b* is a zoom-in of the marked region in *a*.

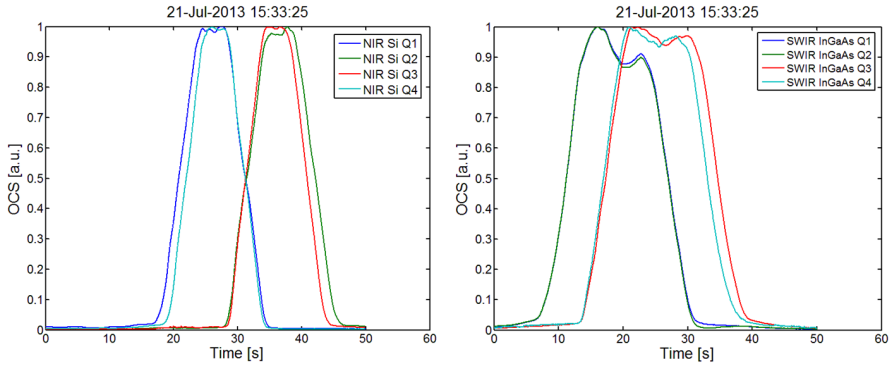

Figure 4.3: Result of weighting the segments as they initially might be amplified differently.

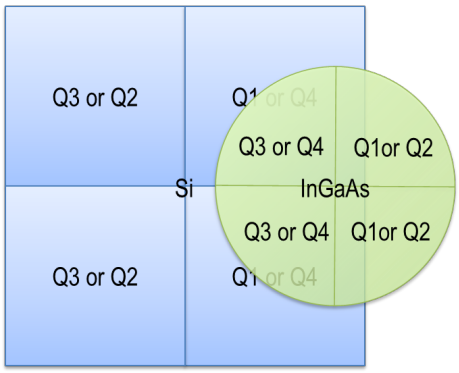

Figure 4.4: First orientation suggestion.

Now, as the uneven amplification of the segments of each quadrant have been compensated for, the next step is to get the correct value of the intensity, expressed in mm^2. The white references are the white spheres as mentioned in chapter 3.7.1 which are used to get the correct conversion constant for the signal so one can get the OCS of a detected item. As the sphere does not enter all four segments equally it can be somewhat tricky to determine this constant perfectly. The method used is quite simple. By integrating over the signal and fitting a square pulse to the signal of the same area and the width of the FWHM, a certain height of the square pulse[1] is obtained. In figure 4.5 the fit is shown for each segment of both quadrants. The segment signals which do not make it over a certain threshold will be neglected. The signals large enough to make it, will then be used to calculate a mean value. This calibration procedure will be done with all six sphere in order to get an overall mean conversion coefficient. This leads to a calibration event with the OCS in mm^2 on the vertical axis, see figure 4.6. When this calibration is done, the OCS is obtained for the pendulum observed both with the Si and the InGaAs quadrant. Notice that the pendulum appears smaller with the Si quadrant, about $1000mm^2$ compared to InGaAs quadrant which is $1600mm^2$. The size of the pendulum in the different spectral regions will be used to adjust the conversion constant for the quadrants for different times of the day[2].

[1] The slope of the pulse signal can be seen as a measure of how much in focus the detected dropped sphere is. In focus the sphere should generate a square pulse at detection and the further away, it becomes more of a Gaussian shape.

[2] As the position and intensity of the light source used changes throughout the day, the intensity of an insect is different depending on the time of the day.

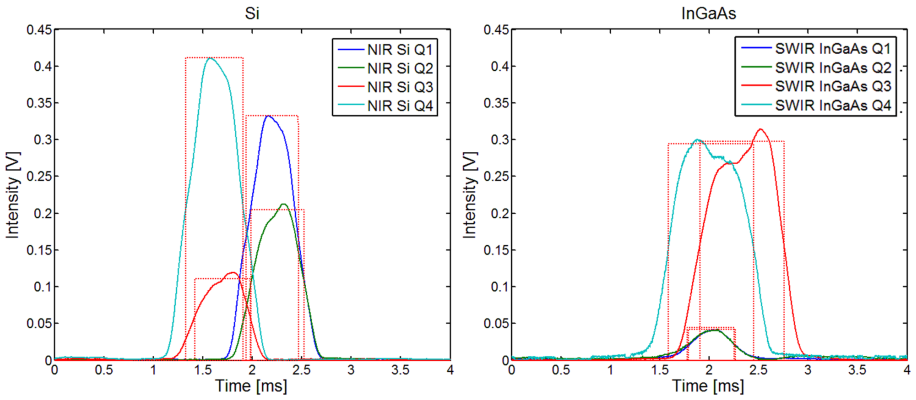

Figure 4.5: A square signal is fitted to each segment signal.

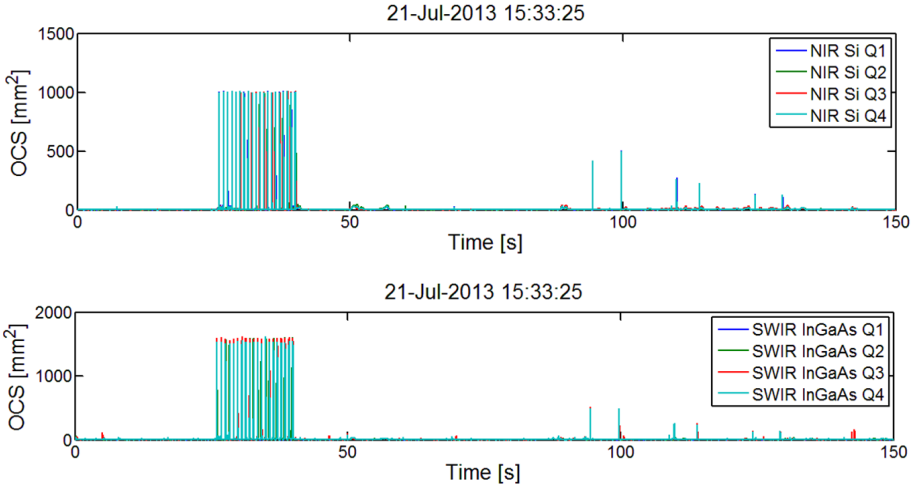

Figure 4.6: Calibration event with the true OCS in mm^2. The size of the spheres are about $490mm^2$, $254mm^2$ and $113mm^2$.

When observing figure 4.5 again, we can learn more considering the orientation of the quadrants which we are not fully familiar with. The signals from the Si quadrant are all unequal while the InGaAs 3 and 4 are the same and 1 and 2 as well, looking at the intensity. In the case of Si it seems like the quadrant should be somewhat tilted as the sphere initially falls through seqment 3 and 4, largest part of the sphere entering segment 4 while when it falls through 1 and 2 there is a more equal part of the sphere visible in both segments. From this, the position of the quadrants can be determined, assuming that the sphere is falling straight downwards. For the InGaAs quadrant the case is different,

the sphere appears to fall through the FOV of segment 3 and 4 mostly with some time difference. Segment 1 and 2 are entered at the same time, equally as little. As 3 is entered first, the 1 and 2 just a little bit at the same time and then 4 the orientation of the quadrant has to be rotated $\pi/4$ compared to the Si quadrant. A new suggestion of the orientation is given, see figure 4.7.

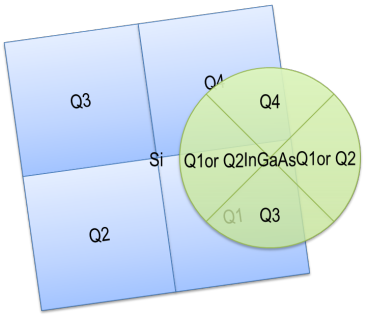

Figure 4.7: Second orientation suggestion.

This suggestion contradicts the first suggestion considering the InGaAs quadrant. As the matter is examined it appears that some electronic malfunction caused two segments (1 and 2) to short circuit. By further investigation of figure 4.5, the segment 1 and 2 of InGaAs are entered at the same time as segment 4, therefor the final quadrant orientation is presented in figure 4.8.

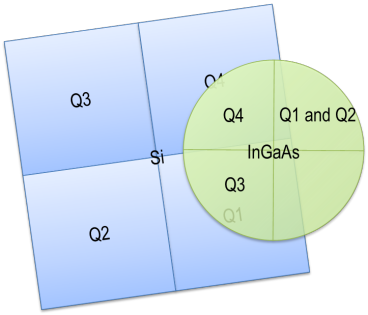

Figure 4.8: Final segment orientations.

The form factor of the system was determined by using the pendulum as during calibrations, but at different distances from LUMBO. The series of pendulum events can be seen in figure 4.9. Note that the FOV was entered when moving and adjusting the pendulum in order for it to enter the FOV properly. As the sequence of measurements was documented, the relative intensity of the signal can be displayed as a range dependent signal. Using the form factor equation from chapter 2.5 the experimental data can be compared with the

theoretical data, the result can be seen in figure 4.10.

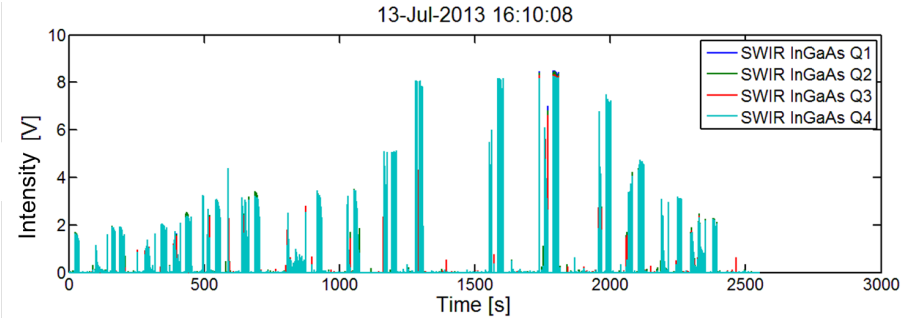

Figure 4.9: Form factor calibration sequence.

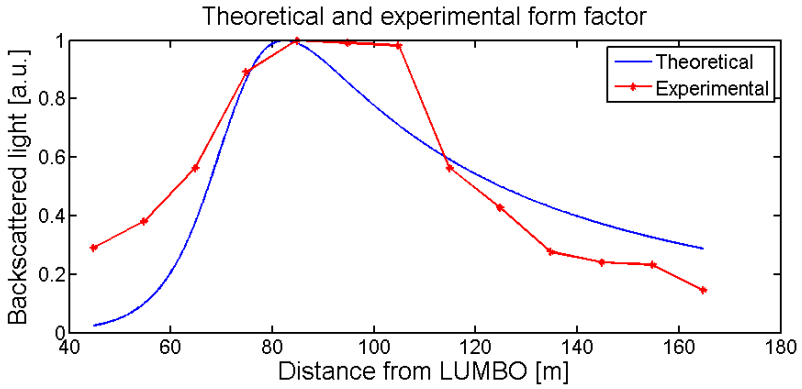

Figure 4.10: The theoretical form factor compared with the experimental one.

4.2 Camera recordings

In order to find images of insects flying through the FOV and also reflected in the mirror, the easiest way is to write an algorithm that searches through the images in a folder automatically. But it seems to be quite hard to do as the mirrored image of the insect usually becomes very weak and therefor is eroded when thresholding the image. The fact that the mirror is not entirely static makes it also a bit complicated. But as the controlled insect releases are of a finite number, the images are searched through manually. One event is found where a large earth bumble bee (*Bombus Terrestris*) is flying through the FOV and is reflected in the mirror, see figure 4.11. By thresholding the image and extracting the position of the selected object, the direct and mirrored trajectory is imaged in order to get a better overview, see figure 4.12.

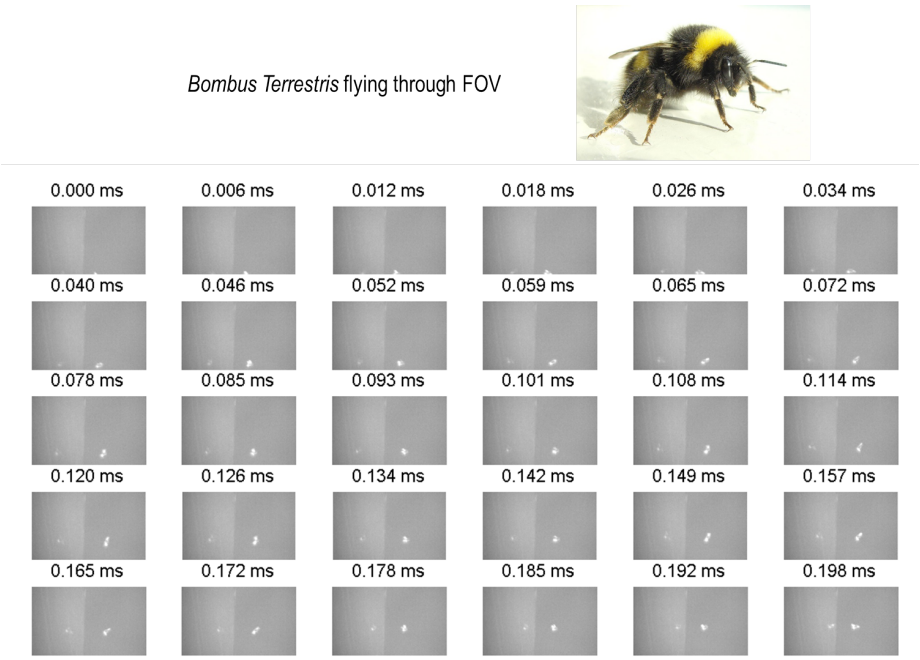

Figure 4.11: Sequence of *Bombus Terrestris* flying through FOV.

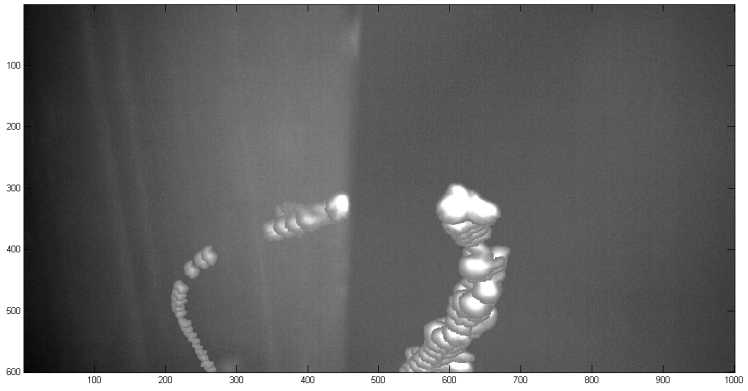

Figure 4.12: Trace of flight, showing the flight trajectory.

For every image the position of the insect in the direct space and in the mirrored one is extracted from the image and plotted as a function of x and y. In figure 4.13 these data points are marked with a time stamp. By knowing from chapter 3.4 how the coordinate system is mirrored we can obtain the

three dimensional insect light path seen in figure 4.14. As the magnification of the image plane can be calculated knowing the camera chip size and the focal length of the telescope used along with it, the coordinate axes can be determined correctly.

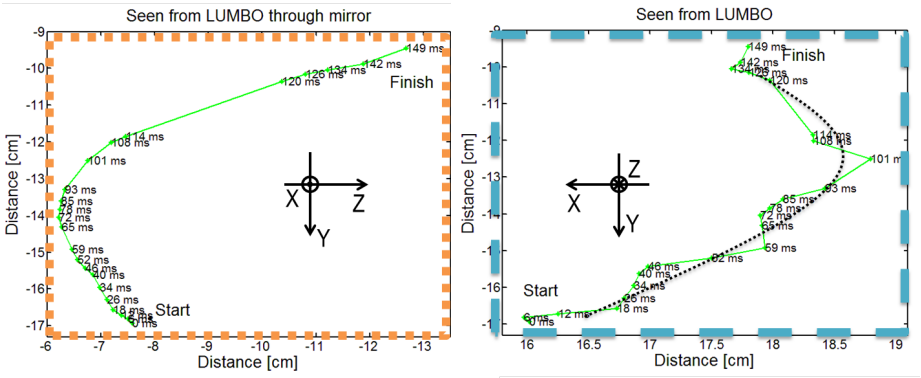

Figure 4.13: Calibrated flight trajectory in z-y and x-y plane.

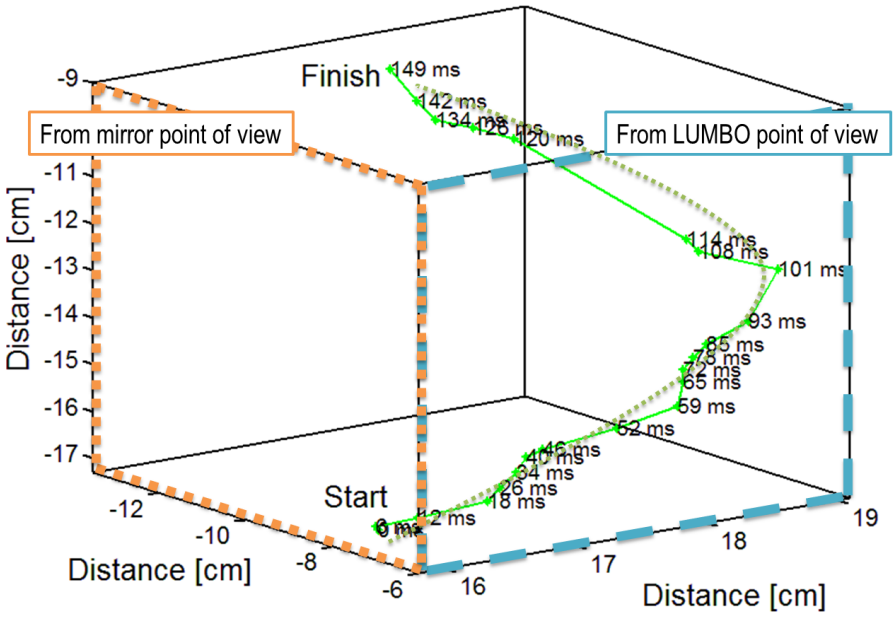

Figure 4.14: Calibrated trajectory in space.

4.2.1 Insect events

As the insect event evaluated in chapter 4.2 is the only event of a captured known insect which is visible in the mirror too, this event is found in the quadrant data. It seems like the insect has only been detected by the InGaAs quadrant, by segment 1, 2 and 4[3], see figure 4.15. As the insect is both in FOV and mirrored at the same time for a very short period of time there is a very small chance that the quadrant data is from that part. Therefore some other insect events are investigated and the evaluation will be done a bit differently compared to figure 3.14. Initially the idea was to get the prediction of flight direction from the camera image sequence and the harmonic frequency content from the quadrant, in order to determine the insect specific model A. Instead an insect event will be investigated and a flight direction will be proposed according to the insect model described in chapter 2.4, as the true flight direction is not known from any high speed camera sequence.

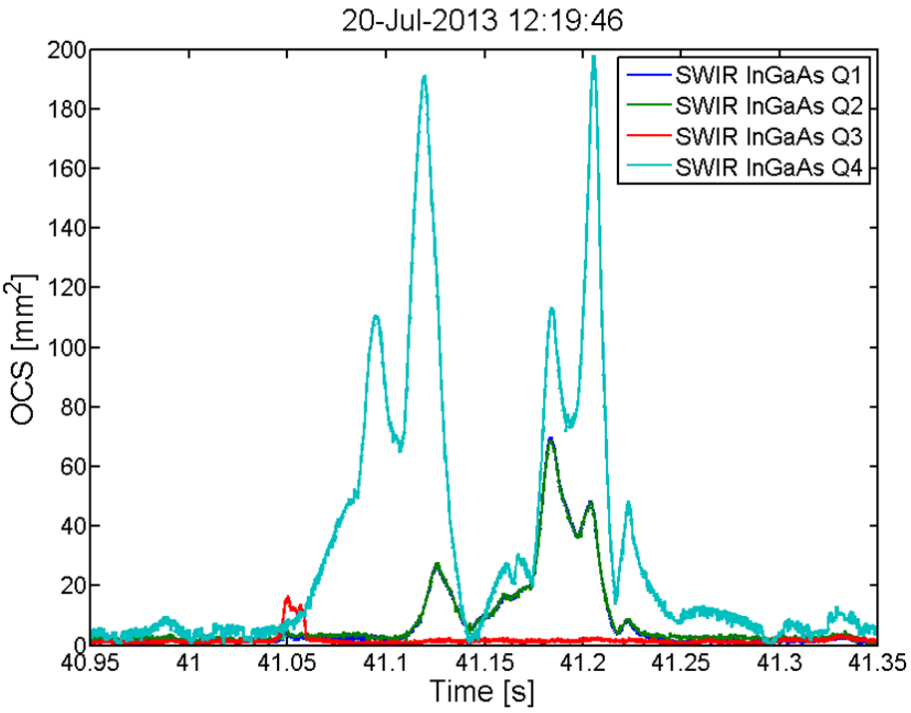

Figure 4.15: *Bombus Terrestris* flying through the FOV of the InGaAs quadrant, insect is also mentioned in section 4.2.

In figure 4.16 an interesting insect event is shown. The modulation pattern seems to change with time, looking at segment 4 of the InGaAs quadrant. As it is

[3]Known from previous evaluation of calibration events, segment 1 and 2 of the InGaAs quadrant always shows exactly the same signal.

zoomed in on, we can also see a fascinating yet not too surprising phenomena. The pattern of the modulation appears somewhat different for the different quadrants, see figure 4.17.

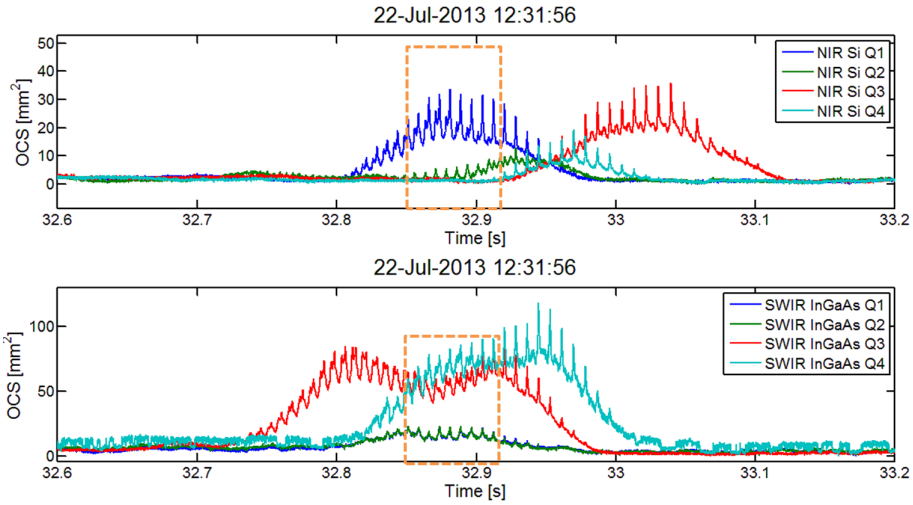

Figure 4.16: An insect event seen with both the Si and the InGaAs quadrant.

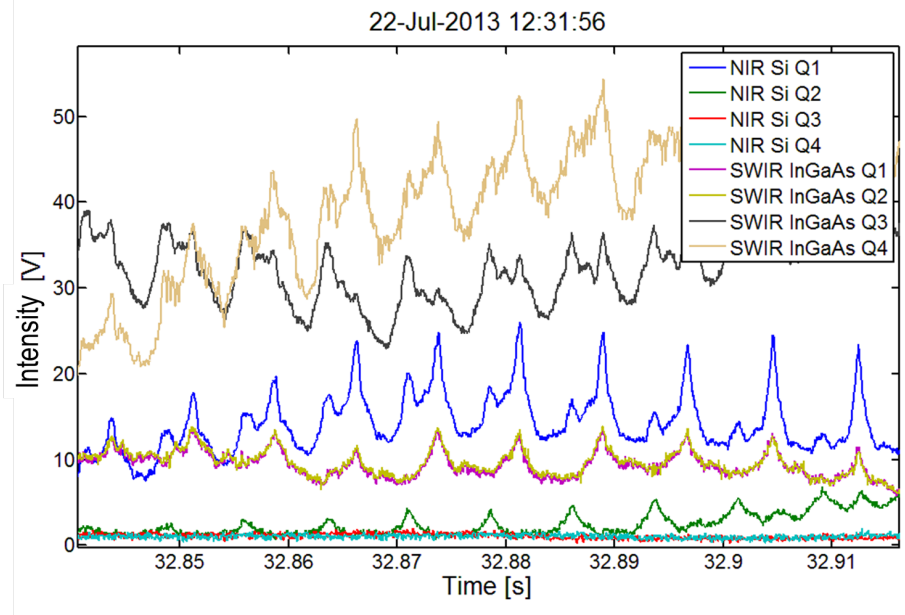

Figure 4.17: Figure 4.16 zoomed in at the selected area.

A spectrogram of a file containing the insect event is done according to theory in chapter 3.7.2, see figure 4.18. As time passes each event is imaged and the color tells the relative intensity of each frequency component. Figure 4.19 is a zoom-in of previous spectrogram, here three insect events are shown, where the differences in body size and frequency is obvious. By extracting one spectrum along the vertical axis of an insect event one can see the differences even more clear than before, see the spectrum for the three clear insect events in figure 4.20. Insect 2 is the one which was examined previously in figure 4.16 and 4.17.

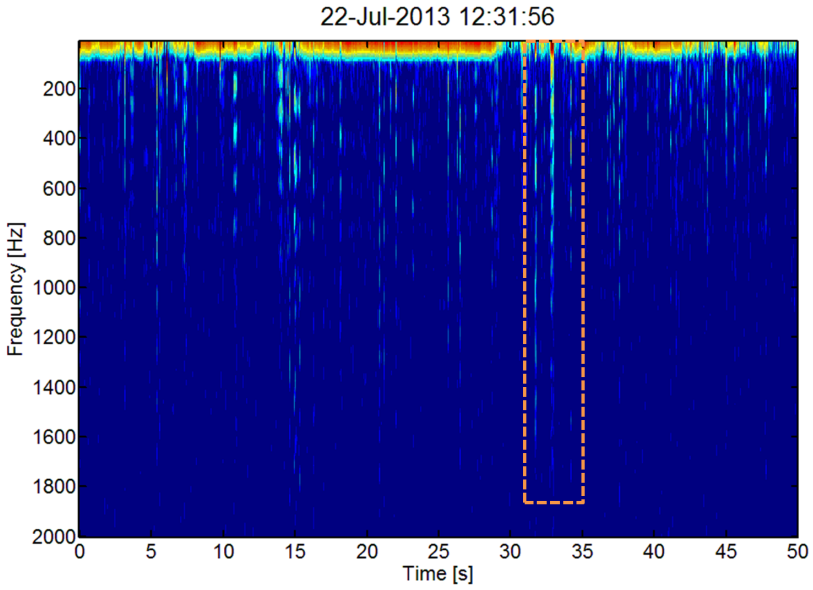

Figure 4.18: A spectrogram of the file containing three insect events that will be further investigated, these are located inside the marked region.

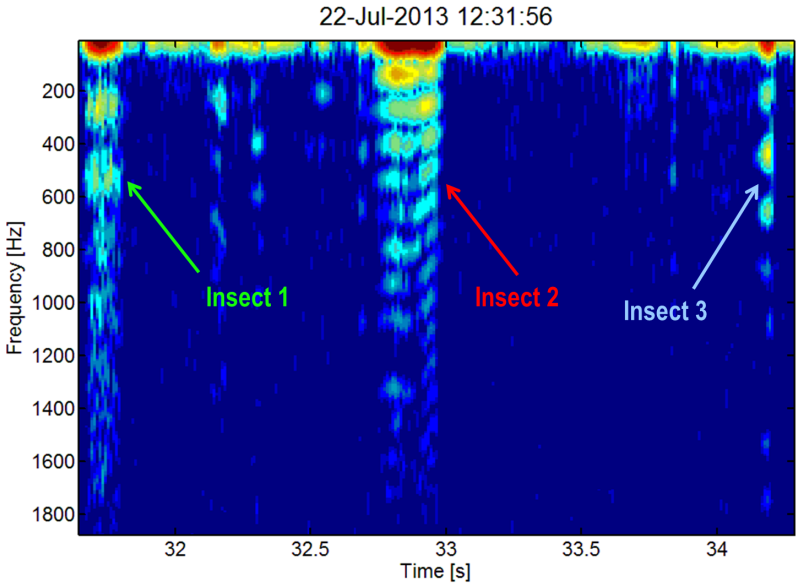

Figure 4.19: The marked region of the spectrogram in figure 4.18.

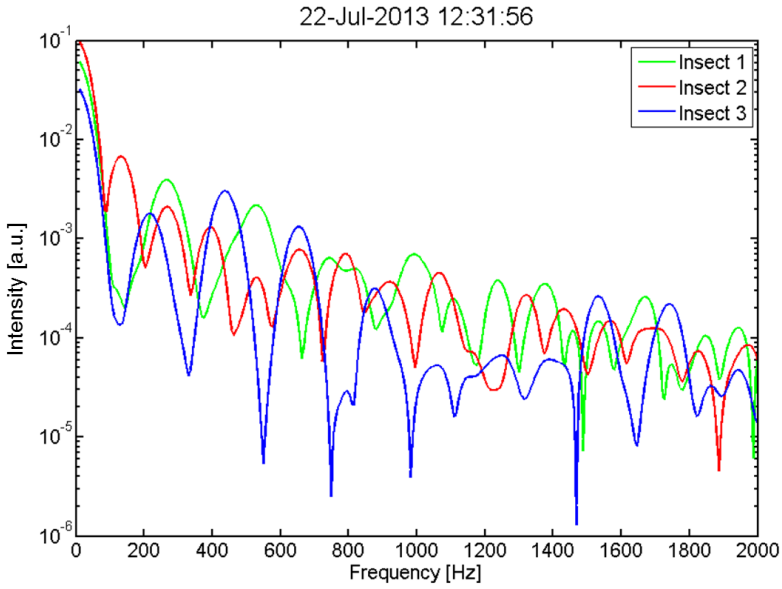

Figure 4.20: The frequency of the three chosen insect events in previous figure.

4.3 Insect model implementation

To extract information about the flight direction, the insect model presented in chapter 2.4 should be considered and applied to, in order to identify the flight direction of the three insects in the spectrogram in figure 4.19 and spectrum in figure 4.20. From the insect model it is known that the OCS depends on the angle of observation. From the side, one would observe a strong 2ω but from the front a strong 1ω would be observed. The change of the relative intensity of the two frequency components could be of interest in order to detect change of flight direction and eventually the exact direction of flight. Figure 4.21, 4.22 and 4.23 shows the insect event 1, 2 and 3 along with the phase difference between the first even and odd harmonics and the relative intensity of the first even and odd harmonics.

The first two insect event results in similar appearances, in both the relative intensity of the harmonics as well as in the phase difference. For insect 1 there seems to be a change of phase difference and also a change in relative intensity between the first odd and even harmonics at the same time. For insect 2 there seems to be a change of relative intensity just as the phase difference increases again after some decreasing. In the case of insect 3 it is hard to interpret the situation as it differs a lot from the previous two, and also the duration of the event is short. The case might be, that there is no change in relative intensity and phase difference, but this is hard to see due to the fluctuations of the signal. By looking at the actual insect signal, the modulation pattern seems not to change at all during the event. The three insects are evaluated in table 4.1.

Insect	Relative Intensity	Phase difference, $\Delta\phi$
1	t=31.65-31.705: strong 1ω t=31.705-31.8: strong 2ω	at t=31.705: $\Delta\phi$= -125 degrees
2	t=32.72-32.8: strong 1ω t=32.8-33: strong 2ω	at t=32.8: $\Delta\phi$= -60 degrees
3	t=34.14-34.21: stronger 2ω than 1ω	at t=34.14-34.21: $\Delta\phi$= 0

Table 4.1: Evaluation of the three insect events.

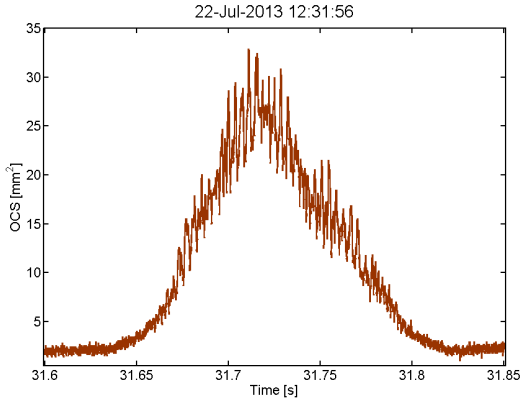

(a) Signal.

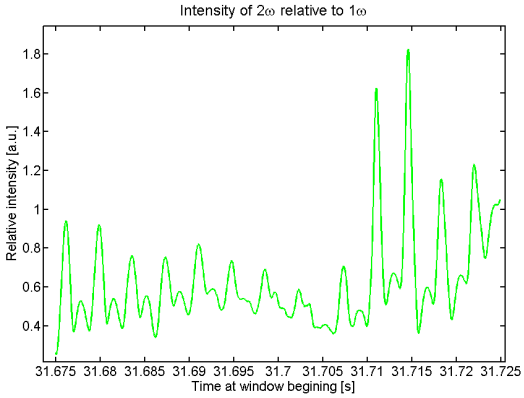

(b) ΔIntensity.

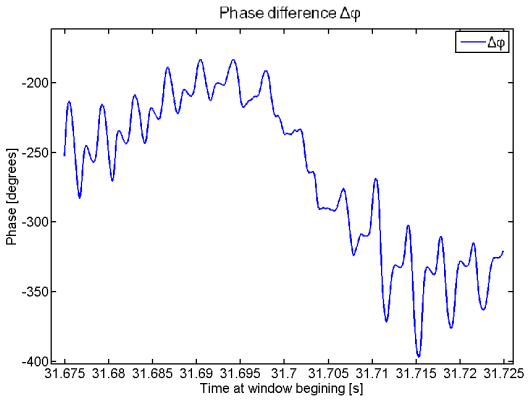

(c) $\Delta\phi$.

Figure 4.21: The signal, the relative intensity and the phase difference $\Delta\phi$ of insect 1.

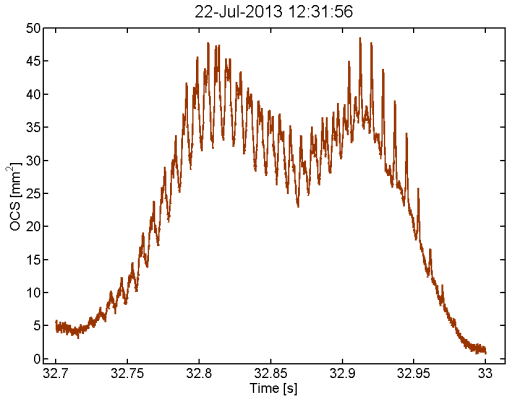

(a) Signal.

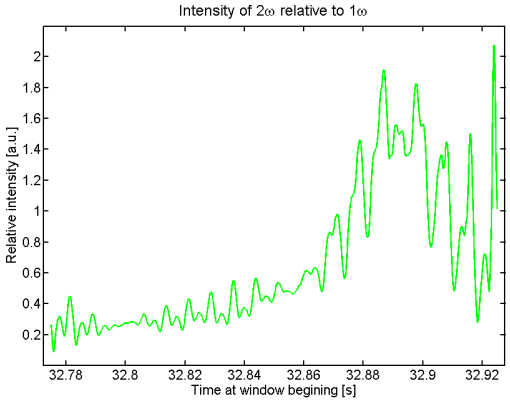

(b) ΔIntensity.

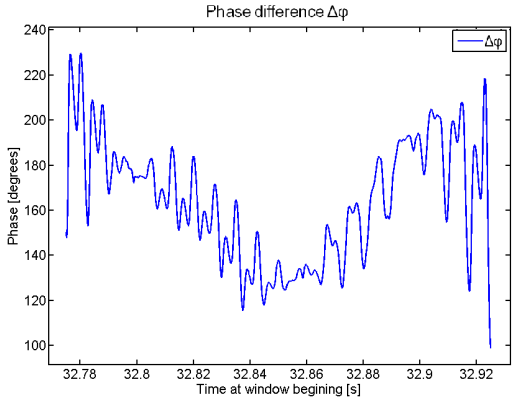

(c) $\Delta\phi$.

Figure 4.22: The signal, the relative intensity and the phase difference $\Delta\phi$ of insect 2.

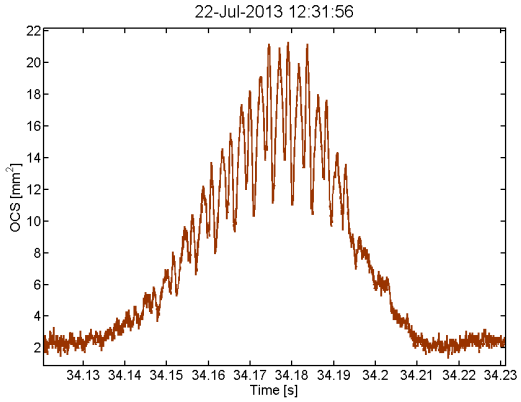

(a) Signal.

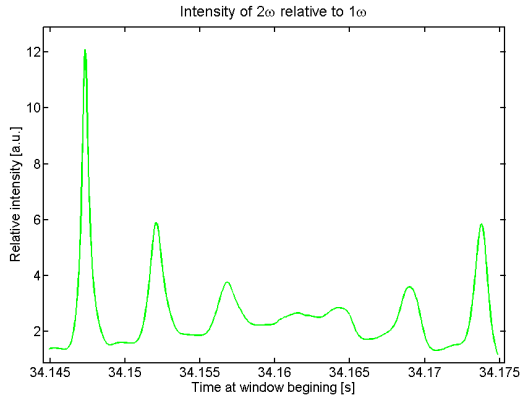

(b) ΔIntensity.

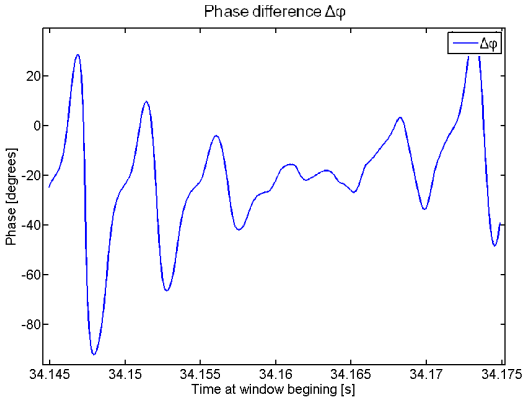

(c) $\Delta\phi$.

Figure 4.23: The signal, the relative intensity and the phase difference $\Delta\phi$ of insect 3.

The oscillation present in the figures displaying the relative intensity and the phase difference is not fully identified, but some aspects of the data evaluation that might be possible causes of this is presented in chapter 4.4.

4.4 Error sources

- InGaAs quadrant shows the same signal for segment 1 and 2 meaning that the pixels are merged together due to electronic malfunction. This results in the InGaAs quadrant providing 3-pixle information.
- During evaluation of the frequency components in the insect events in chapter 4.3 a sliding window was applied in order to obtain the changes in relative intensity and the phase difference during the entire event. As the window was swept over the signal, it was noticed that the frequency bins would sometimes change depending on which part of the signal it showed. As the bins were chosen in advance, this might lead to some error in the data concerning the phase and intensity information of the interesting frequency components of the signal.

Chapter 5

Conclusion

With a versatile scientific facility such as the Lund University Mobile Biosphere Observatory (LUMBO), the possibilities of both active and passive remote sensing is a great asset for scientists doing research on insects. By getting access to the huge amount of information which is offered non-intrusively, good statistics can be obtained. The pilot field campaigns during the summer of 2013 has given an insight to all the possibilities of the platform in the field of biology, entomology and ecology. During an 8 hour work day[1] LUMBO registers approximately 20 000 insect events in an air volume of $1m^2$ (for a InGaAs quadrant), containing information about *a*) backscattered light in two spectral bands, NIR and SWIR; *b*) color information in the visible range; *c*) weather data and *d*) high speed camera recordings. Correlating the information of wingbeat frequency, wingbeat pattern, body size, wing size and color, which is information that can be extracted from the data $a - d$, these parameters can be used to eventually categorize insects into species, gender and age. When such categorization is done, other information such as behavior of specific type of individuals can be examined. By being able to correlate the direction of flight and the information about the spatial separation between certain individuals, interaction between individuals of different genders, or perhaps between predator and pray can be analyzed. Also the behavior of insects relative to other external factors can be studied, such as the insect activity relative to the weather, food, other animals, or perhaps relative to the time of the year.

The determination of direction of flight by analyzing the backscattered light from insects has been of main interest. The initial idea of obtaining the true direction of flight from high speed camera and by the use of a tilted mirror, is rejected as no sufficient image data along with matched quadrant data was obtained. A better mirror which is angled more should be a sufficient way of increasing the chance of recording good insect flight image sequences. Nevertheless, three insect events were chosen and the ability to obtain information about possible change of flight direction is examined by

[1] LUMBO also operates during night time, running LIDAR measurements.

analyzing the time dependent phase and relative intensity information of the harmonic frequency components.

Finally, the direction of flight is not possible to determine, but, flight direction changes are shown. This change can in some cases be seen with the naked eye when observing the modulated quadrant signal of an insect event, which changes with time. This kind of observation has previously been mentioned by *A. Moore (1981)*, who concluded that the orientation of the insect was one of the reason for within-species variation of the waveform, causing limitation of insect identification.

With further research perhaps an insect specific model that describes the three dimensional time dependent OCS of a certain type of insect, can be used to do more exact research about specific insect species.

5.1 Future work

Throughout this thesis, there has been change of plans due to delayed shippings, weather, technical issues, bad luck and some non cooperating insects. Learning from all unexpected changes (both to the good and the bad) a few points will be addressed in order for future field campaigns to be successful.

- Black flute plastic is a great material for the construction of a termination cavity. The shape of the terminator was modified when adding a tilted piece of loose plastic inside it and by adding a cape which successfully improved the darkness of the terminator. Another shape might be something that could improve the function of the terminator, perhaps Wood's horn [22] which is a long bent horn would be worth considering.

- When the form factor of the system is measured, it would be interesting to also investigate the change of signal steepness as for example the pendulum, as it moves towards and away from focus. In this way the focus adjustments can be done in order to obtain sharper signals.

- In order to obtain an OCS expressed with the insect specific model A, which gives a good description of insects in all angles, experiments should initially be done in laboratory. This could be done with a very simple setup, similar to the one mentioned earlier in this thesis with the clear plastic cookie jar made by *A. Moore (1981)* (section 1.1), but with complementary three dimensional imaging equipment.

- The wind can influence the flight trajectory of an insect by making it fly in one direction, even though it is not oriented in that way. This means that if one only takes the orientation of the insect body into account in order to obtain the flight direction, it might be wrong. Then on the other hand one can discuss if the intended or the net flight direction is the more interesting one. Either way, the fact that a four pixel photodiode is used, it can be used to indicate whether the direction is as detected or not, as long as the orientation of the diode is known.

- The spatial alignment of the telescopes should be done with someone on the distance of interest with walkie-talkie communication in order to do calibration and achieve an overlap of the FOVs of interest.
- If using a calibration box with a tilted mirror, 3D calibration should be done in order to obtain the tilt of the mirror and so the correct 3D trajectory can be extracted from a 2D image. 3D calibration can be done by inserting a b/w checkerboard in the FOV and move it around. This matter should be investigated further as it was not further investigated in this thesis.
- When evaluating the calibration events in order to obtain the time dependent conversion constant from V to the OCS in mm^2 which is done in section 4.1.1, there are many ways to go through with it. Depending on how the data of the quadrant segments are evaluated, one can argue which method (e.g. max, mean, median) is the best.

Appendix A

Spherical harmonics

The spherical harmonics is the angular part of the solution of the Laplace's equation expressed in spherical coordinates, usually written as $Y_l^m(\theta, \phi)$ and expressed as in equation A.1 where P_l^m is the associated Legendre polynomials.

$$Y(\theta, \phi) = \Theta(\theta)\Phi(\phi) = \sqrt{\frac{2l+1}{4\pi}\frac{(l-m)!}{(l+m)!}}P_l^m(cos\theta)e^{im\phi} \tag{A.1}$$

The function where l is a positive integer and where $m = -l, -(l-1), .., l-1, l$ will be a complete set of base functions on the unit circle, meaning that using the spherical harmonics one can use them to build any function $f(\theta, \phi)$ on a sphere as expressed in equation A.2 where $a_{m,n}$ is the normalization constant [29, 30].

$$f(\theta, \phi) = \sum_{m,n} a_{m,n} Y_n^m(\theta, \phi) \tag{A.2}$$

The spherical harmonics consist of a real and an imaginary part, for $l = 0, 1, 2$ are shown in figure A.1 the real part of the function is presented, visualized using the MATLAB script *spharm4* which is available for usage on *mathworks.com*. As noticed in the figure the functions where l is even there exists a certain symmetry whilst when l is odd there is not.

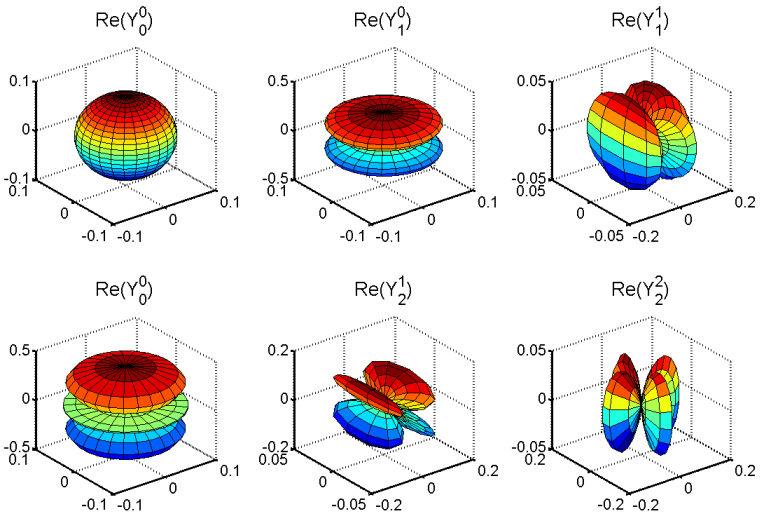

Figure A.1: The first real spherical harmonics.

Bibliography

[1] I. R. Richards. Photoelectric cell observations of insects in flight. *Nature*, 175(4446):128–129, 1955.

[2] A. Moore and R. H. Miller. Automated identification of optically sensed aphid (homoptera: Aphidae) wingbeat waveforms. *Entomological Society of America*, 95:1–8, 2002.

[3] David S. Hoffman, Amin R. Nehrir, Kevin S. Repasky, Joseph A. Shaw, and John L. Carlsten. Range-resolved optical detection of honeybees by use of wing-beat modulation of scattered light for locating land mines. *Applied Optics*, 46(15):3007–3012, 2007.

[4] Kevin S. Repasky, Joseph A. Shaw, Ryan Scheppele, Christopher Melton, John L. Carsten, and Lee H. Spangler. Optical detection of honeybees by use of wing-beat modulation of scattered laser light for locating explosives and land mines. *Applied Optics*, 45(8):1839–1843, 2006.

[5] William G. Evans. Infra-red receptors in melanophila acuminata degeer. *Nature*, 202(4928):211, 1964.

[6] Eric Warrant and Dan-Eric Nilsson. *Invertebrate Vision*. Cambridge University Press, 978-0521830881, 1st edition, 2006.

[7] Anna Runemark, Maren Wellenreuther, Hiran H. E. Jayaweera, Sune Svanberg, and Mikkel Brydegaard. Rare events in remote dark-field spectroscopy: An ecological case study of insects. *IEEE Journal of Selected Topics In Quantum Mechanics*, 18(5):1573–1582, 2012.

[8] Faculty of Engineering. Fluoresence lidar. `http://www.atomic.physics.lu.se/research/applied_molecular_spectroscopy_and_remote_sensing/research_overview/fluorescence_lidar/`, 2012.

[9] Google. Maps. `https://maps.google.se`, 2013.

[10] Sune Svanberg. *Atomic and Molecular Spectroscopy*. Springer, 3-540-20382-6, 4th edition, 2004.

[11] Mikkel Brydegaard. *Aspects of Optical Broad Band Spectroscopy and Information Extraction - Applications in Medicine and Ecology.* 978-91-7473-353-2, 2012. Doktoral thesis, Lund University.

[12] Wolfram Alpha. Sun. `http://www.wolframalpha.com/input/?i=sun`, 2013.

[13] Maggy Sikulu, Gerry F Killeen, Leon E Hugo, Peter A Ryan, Kayla M Dowell, Robert A Wirtz, Sarah J. Moore, and Floyd E. Dowell. Near-infrared spectroscopy as a complementary age grading and species identification tool for african malaria vectors. *Parasites & Vectors*, 43(3), 2010.

[14] Maren Wellenreuthe. Personal communication. `http://marenwellenreuther.com/`, 2013.

[15] Lauren J. Cator, Alongkot Ponlawat Benjamin J. Athur, and Laura C. Harrington. Behavioral observations and sound recordings of free-flight mating swarms of ae. aegypti (diptera: Culicidae) in thailand. *Journal of Medical Entomology*, 48(4):941–946, 2011.

[16] WHO. World malaria report 2012 summary. `http://www.who.int/malaria/publications/world_malaria_report_2012/wmr2012_summary_en.pdf`, 2013. pdf.

[17] Ekaterina Shevtsova, Christer Hansson, Daniel H. Janzen, and Jostein Kjaerandsen. Stable structural color patterns displayed on transparent insect wings. *Proceedings of the National Academy of Sciences of the United States of America*, pages 668–673, 2010.

[18] Philip Ball. Flight of the bumblebee decoded. `http://www.nature.com/news/flight-of-the-bumblebee-decoded-1.13587`, 2013.

[19] Claus Weitkamp. *Lidar: Range-Resolved Optical Remote Sensing of the Atmosphere.* Springer, 978-0-387-40075-4, 2005.

[20] Hiroaki Kuze, Hideki Kinjo, Yasushi Sakurada, and Nobou Takeuchi. Field-of-view dependence of lidar signals by use of newtonian and cassegrainian telescopes. *Applied Optics*, 37(15):3128–3132, 1998.

[21] B.E.A. Saleh. *Fundamentals of Photonics.* John Wiley & Sons, 978-0-471-35832-9, 2nd edition, 2007.

[22] Philip C. D. Hobbs. *Building Electro-Optical Systems, Making It All Work.* John Wiley & Sons Inc, 978-0-470-40229-0, 2000.

[23] A. Drake. *Radar Entomology, Observing Insects Flight and Migration.* Cabi international, 978-1-84593-556-6, 2012.

[24] Hamamatsu. Infrared detectors. `http://www.hamamatsu.com/resources/pdf/ssd/infrared_kird0001e.pdf`, 2013. pdf.

[25] François Blais. Review of 20 years of range sensor development. *Journal of Electronic Imaging*, 13(231):62–76, 2004.

[26] Sanjit K. Mitra. *Digital Signal Processing, A Computer-Based Approach*. McGraw-Hill, 0-07-232105-9, 2nd edition, 2001.

[27] Matlab. Documentation center. `http://www.mathworks.se/help/matlab/index.html`, 2013.

[28] David S. Watkins. *Fundamentals of Matrix Computations*. Wiley-Interscience, 0-471-21394-2, 2002.

[29] WolframAlpha. Spherical harmonics. `http://www.wolframalpha.com/input/?i=spherical+harmonics`, 2013.

[30] Ulf Torkelsson. Associerade legendre-funktioner och klotytefunktioner. Technical report, Chalmers tekniska högskola, 2009.